10159
NACA TN 3806

TECH LIBRARY KAFB, NM
0066718

NATIONAL ADVISORY COMMITTEE FOR AERONAUTICS

TECHNICAL NOTE 3806

COMPARISON OF NACA 65-SERIES COMPRESSOR-BLADE PRESSURE DISTRIBUTIONS AND PERFORMANCE IN A ROTOR AND IN CASCADE

By Willard R. Westphal and William R. Godwin

Langley Aeronautical Laboratory
Langley Field, Va.

Washington
March 1957

AFMDC
TECHNICAL LIBRARY
AFL 2811

TECH LIBRARY KAFB, NM
0066718

3

NATIONAL ADVISORY COMMITTEE FOR AERONAUTI

TECHNICAL NOTE 3806

COMPARISON OF NACA 65-SERIES COMPRESSOR-BLADE PRESSURE DISTRIBUTIONS AND PERFORMANCE IN A ROTOR AND IN CASCADE[1]

By Willard R. Westphal and William R. Godwin

SUMMARY

An investigation has been conducted to compare the performance of NACA 65-series compressor blades in two-dimensional cascade with that in an axial-flow compressor. The entering and leaving flow velocities, pressure rise, and the pressure distribution on the rotating blades were measured at three radial stations of a free-vortex rotor. The blade pressure distributions were obtained by the use of a mercury-seal pressure-transfer device. The data obtained were compared with similar data for the same blade sections obtained from a two-dimensional porous-wall cascade tunnel.

The comparison indicated that cascade data accurately predicted the turning angle and blade pressure distribution obtained in the compressor at design conditions. At other than design angle of attack, large differences, probably due to secondary flows, were observed near the inner casing.

INTRODUCTION

A prime factor in the design of a turbomachine is the knowledge of rotor-blade aerodynamic performance. However, blade profiles may be tested and evaluated much more easily in cascade than in a rotating machine since models are simpler and compressor design parameters, such as blade camber and solidity, are more easily varied in the cascade. Also, the section characteristics such as lift, drag, and pressure distribution are more easily measured in cascade. Unfortunately, flow through a two-dimensional cascade is somewhat different from that through a rotating machine since such three-dimensional phenomena as radial displacement of the main flow, centrifuging of the boundary layer, and the tip clearance leakage do not occur in cascades. A correlation is needed between

[1]Supersedes recently declassified NACA Research Memorandum L51H20 by Willard R. Westphal and William R. Godwin, 1951.

the simpler two-dimensional cascade flows and the flows through rotating blade rows. One method of obtaining information for this correlation is to measure the pressure distributions and flow velocities on rotating blade rows. In reference 1, Weske presented pressure distributions measured on rotating blades, but did not present cascade data for comparison. In reference 2, Mühlemann presented flow velocity measurements ahead of and behind a rotor, along with blade wake distributions. As in the previous case, comparable cascade data were not presented; so a correlation between rotor and cascade performances could not be attained.

The intent of the present investigation was to obtain a comparison between the flow about compressor-blade sections in a compressor rotor and in two-dimensional cascade. An axial-flow compressor consisting of guide vanes and a rotor was used. The rotor blades were constructed with NACA 65-series 10-percent-thick airfoil sections, for which cascade data were available. The cascade data were obtained in porous-wall cascades which closely approximate two-dimensional-flow conditions by removing the boundary layer from the walls enclosing the blade row. A more extensive discussion of porous-wall cascades can be found in reference 3. The porous-wall cascade data were taken from reference 4. In order to determine the manner in which the cascade and rotating blade flows differed, blade surface pressure distributions and entering and leaving velocities were measured at three radial positions in the test compressor. The measurement of pressures on the rotating blades was made possible through the use of a pressure-transfer device (ref. 5), which simultaneously transmitted 24 pressures from the rotor to the stationary manometer.

SYMBOLS

c	blade chord, in.
$(c_n)_M$	section normal-force coefficient, from measured changes in momentum and static pressure
$(c_n)_P$	section normal-force coefficient, from integrated pressure distributions
$(c_n)_\theta$	section normal-force coefficient, from ideal change in momentum and static pressure when corrected values of α and θ were used
M	Mach number
p	static pressure, lb/sq ft
H	total pressure, lb/sq ft

q dynamic pressure, lb/sq ft

R Reynolds number

t blade thickness, in.

U rotational velocity of rotor blade at any radius, ft/sec

V velocity of air relative to casing, ft/sec

α angle of attack; angle between entering air and chord line, deg

β inlet air angle; angle between entering air and axial direction, deg

θ turning angle; angle through which the air is turned by the blade element, deg

σ solidity, blade chord divided by gap between blades

ψ yaw angle, deg

Subscripts:

1 entering guide vanes

2 leaving guide vanes

3 entering rotor, relative to rotor

4 leaving rotor, relative to rotor

5 leaving rotor, stationary coordinates

ax axial direction

l local

Stations:

I instrument station ahead of guide vanes

II instrument station between guide vanes and rotor

III instrument station behind rotor

APPARATUS

General arrangement.- The 42-inch tip diameter axial-flow test compressor used in this investigation (fig. 1) contained a single row of guide vanes and a single row of rotor blades. The guide vanes were installed during a previous testing program and were retained to establish a free-vortex flow ahead of the rotor. The entrance and test section of the compressor were enclosed in a frame building. Half the building was mounted on rails and was rolled open to expose the bellmouth inlet of the compressor. The rotor drive motor was a 1,000-horsepower synchronous electric motor supplied by a variable-frequency converter. The general configuration was essentially as described in reference 5, with the exception that the ducting downstream of the first diffuser was replaced by a vane-type throttle valve.

Rotor blades.- A sketch of the rotor blades is shown in figure 2. The blades, 24 in all, were designed to straighten the free-vortex flow leaving the guide vanes into an axial flow. At the design inlet air angle of 60°, constant from root to tip, the ratio of axial velocity to tip speed was 1.08; the axial velocity was constant throughout the blading. NACA 65-series compressor blade sections were used. The blade cambers and angles of attack were determined from the design charts in reference 4. Three blades contained 24 static-pressure orifices each for pressure-distribution measurements. The orifices were located at the outboard, mean, and inboard sections. The outboard and inboard sections were located 1 inch from the ends of the blades to avoid the wall boundary layer. The blades had a span of 6.5 inches, a constant chord of 5.5 inches, and thus an aspect ratio of 1.182. The blade clearance at the tip was about 0.030 inch. The blade sections tested are described in the following table:

	Outboard	Mean	Inboard
Design lift coefficient. .	1.096	1.200	1.304
Solidity	1.050	1.183	1.355
Blade angle, deg	48.1	46.1	44.7
t/c.	0.10	0.10	0.10

The blade angle is measured between chord line and axis of rotation. Vector diagrams to scale for typical design conditions are shown in figure 3.

Guide vanes.- The row of guide vanes contained 37 blades; each had a span of 6.5 inches and a constant chord of 4 inches. The guide vanes produced a free-vortex velocity profile at station II as shown by the

turning-angle comparison in figure 4. The angles were measured in the uniform flow between adjacent guide-vane wakes. The prewhirl is against the direction of rotation of the rotor, contrary to conventional axial-flow compressor practice.

Pressure-transfer device.- The pressure-transfer device used in reference 5 was not completely satisfactory in that mercury escaped through the pressure leads and caused erroneous readings. A transparent plastic model of one cell of the transfer device was built to determine the cause of the difficulty. By running this model at various speeds with various amounts of mercury, it was found that the mercury splashed only at low rotor speeds or with too much mercury in the cell. This splashing was eliminated by introducing the mercury into the transfer device after the rotor was started and draining the transfer device before stopping the rotor. The 24-cell transfer device was then modified so that the mercury could be introduced into each cell under pressure while the rotor was running and drained before stopping. As further protection against mercury entering the pressure leads, small glass reservoirs were connected to the leads between the transfer device and manometer board. After these changes were made, no further trouble was experienced with the transfer device.

Instrumentation and flow measurements.- Total pressure, static pressure, and flow direction were measured at three survey stations (fig. 1(b)) with instruments of the type shown in figure 5(b). At each of these stations, surveys could be made in a radial direction. In addition, the instrument between the guide vanes and the rotor could be traversed circumferentially as well as radially.

Survey instruments were calibrated in a 15-inch-diameter calibration tunnel and are accurate in yaw angle to $\pm 0.2^{\circ}$ and in static pressure to ± 0.3 percent of the impact pressure when mounted in a uniform stream. No correction to the total pressure was necessary. The static pressure indicated by the instrument was higher than true static pressure. A typical calibration curve is shown in figure 6.

In the course of the investigation, it was found that at certain angles of attack the wakes of the guide vanes impinged on the instrument located behind the rotor (station III); thus, erroneous readings were caused. This source of error was minimized by installing another identical instrument in the same plane but one and one-half guide-vane spacings away circumferentially and considering the data from the instrument which indicated the higher total pressure to be correct.

METHOD OF TESTING

Blade pressure distribution, total pressure, static pressure, and flow direction ahead of and behind the rotor were measured at nine angles of attack, at the outboard, mean, and inboard sections at each of four speeds, 800, 900, 1,000, and 1,140 rpm. The angles of attack at the mean

diameter were varied from 9° up to the stall point by throttling the discharge. All pressure measurements, including the blade pressure distribution at a given blade section, were recorded simultaneously by photographing a multiple-tube manometer board.

For the tuft investigation of the rotor blade passages, nylon tufts were mounted on the blades in rows normal to the flow direction. Five rows were spaced across the blade chord. Each row was mounted on a separate blade so that the air passing over a row of tufts was not affected by any preceding tufts. Tufts were also mounted on the exposed surface of the rotor hub between two adjacent blades. The tufts were observed with the aid of a high-speed stroboscopic light. A contact mounted on the rotor shaft triggered the light at the same instant on each revolution of the shaft. The result, viewed through a port in the outer casing, was a stationary picture of the tufts on one blade as affected by the airstream. By shifting the contactor on the rotor shaft, the other rows of tufts were observed. Observations of the tufts were made over the range of angles of attack.

RESULTS AND DISCUSSION

Blade section pressure distributions.- Blade section pressure distributions at the outboard, mean, and inboard sections at varying mass flows and constant speed are presented in figure 7. The mass flows and corresponding angles of attack for the three sections are presented in these figures. As the mass flow is reduced from about 1.89 slugs per second, the pressure distributions at all three sections become peaked at the leading edge of the upper surface at the same rate. At a mass flow of about 1.27 slugs per second, all three sections are close to the angle of attack at which they would stall. This condition is shown by the sharpness of the leading-edge pressure peaks and indicates a large adverse pressure gradient conducive to separation. As the mass flow is increased above about 1.89 slugs per second, the pressure distributions at all three sections become peaked at the leading edge of the lower surface; thus, the approach of negative stall is indicated.

An interesting phenomenon shown in these plots is the point of nearly constant pressure coefficient (hence velocity ratio) at about the 20-percent-chord point on the upper surface at all angles of attack and all sections. Examination of pressure distributions obtained from compressor airfoils in low-speed cascade substantiates this phenomenon. The position of constant pressure coefficient or velocity ratio varies from one cascade arrangement to another, but for any given cascade a particular point on the convex surface somewhere between 15 and 25 percent chord from the leading edge maintains the same velocity ratio as the inlet angle is varied. The phenomenon of having a point of constant velocity ratio has not been confirmed at high speed nor for blades other than the NACA 65-series. If this continues to exist under compressible-flow conditions,

it would be possible to determine impact and static pressures in a multistage axial-flow compressor at desired radial stations by orifices located at the proper chordwise position of the stator blades and pitot tubes.

Figure 8 shows the effect of rotor inlet Mach number M_3 and Reynolds number on the pressure distribution for three sections at design angle of attack. It can be seen that over the small range of speed covered by these tests there is little change in the pressure distributions.

The pressure distributions for the end points of the angle of attack, Mach number, and Reynolds number ranges over which the blades were tested are shown in figure 9. The distributions indicate a slight increase in the pressure peaks with Reynolds number for the extreme off-design conditions. Although tufts placed on the blades indicated large radial flows in the boundary layer at the high angles of attack, the pressure distributions at all sections are very much alike.

Pressure distributions measured in the test compressor are compared with those obtained from interpolation of porous-wall cascade data in figure 10. The pressure distribution measured at the outboard section in the blower had a slightly higher peak velocity and greater area than that measured in the cascade. This trend is consistent with the greater turning angle measured in the compressor as is discussed in the turning-angle comparisons. At the mean and inboard sections, good agreement can be observed. The wave observed at the 60-percent-chord point in the convex-surface pressure distributions obtained in the cascade is not present in compressor or theoretical distributions (ref. 6). (In ref. 6, Katzoff and Hannah compared theoretical pressure distributions of the NACA 65-(12)10 blade profile at the design angle of attack at a stagger of 60° for two solidities which bracket design conditions of the rotor at the mean section.)

The wave or bump in the porous-wall cascade pressure distributions is due to a small region of laminar separation which occurs at the transition point from laminar to turbulent flow. Laminar flow was possible because of the low turbulence and low Reynolds numbers (about 250,000) of the cascade tests. This separation does not occur in the test blower because of its higher Reynolds numbers (about 700,000) and higher turbulence level due to the wakes from the guide vanes. At each section, the datum point shown on the trailing edge was obtained from the static pressure measured by the survey instrument behind the blades. The pressure rise measured in the compressor is less than that measured in the cascade tunnel because of the boundary-layer growth on the inner and outer casings. The boundary layer on the cascade walls is removed by surface suction and therefore a high static-pressure rise is obtained.

Comparison of Turning Angles in Compressor and Cascade

Plots of turning against angle of attack from both compressor and cascade data are presented in figure 11. The angles are the true geometric (measured) air angles. Since the cascade tests were run at constant inlet air angles, the cascade data were interpolated to obtain turning-angle values at the same angles of attack and inlet angles as the compressor. Interpolation between blade cambers and solidities was also necessary. In figure 12 the angles presented were obtained from a vector diagram having the measured tangential components and an axial velocity equal to the mean of the measured entering and leaving velocities. This method of correction, which is illustrated by the vector diagram in figure 13, is in common use for determining α, β, and θ when the axial velocity is not constant. Correcting the angles to a condition of constant axial velocity reduced the scatter of the blower test points. Some of the scatter may be attributed to the wind gusts present as the intake of the compressor was outdoors.

At the outboard section, the turning angles measured in the compressor were about 1° greater than predicted from cascade data and the trend was similar except at the lowest angles of attack (fig. 12(a)).

At the rotor-blade mean section, the turning angles measured are very close to those predicted from cascade data except at high angles of attack where the slope of the compressor turning-angle curve is higher and the turning angles are greater than in cascade (fig. 12(b)).

At the inboard section, the turning angle compares well with cascade data only near design conditions ($\beta = 60^{\circ}$, $\alpha = 15.3^{\circ}$). The slope of the compressor turning-angle curve is much greater than that of the cascade curve. To be certain that the high turning angles measured actually occurred and were not caused by instrument errors due to the effect of the guide vane wakes on the instruments at station III, the air angles were also measured by observing a tuft through a transparent port in the outer case. Figure 14 is a plot of the air angle relative to the axis of the rotor measured by the instrument against radial distance. The angles measured by the tuft observations were essentially the same as those measured by the survey instrument. The rapid change in angle from a radius of 16.0 inches to the inner case indicates that the secondary effects due to the boundary layer extend beyond the inboard measuring station which is at a radius of 15.5 inches. No information is available on the effect of the case boundary layer on the blade pressure distribution or turning angle. An analysis of main stream and blade boundary-layer flow and their probable effect on the turning angle at the inboard section of the blade follows.

Considering the flow entering the rotor when the compressor is operating at design conditions, the tangential velocity components of the main flow are approximately equal in magnitude to the tangential velocity of the rotor although they are in opposite directions. Thus the radial pressure gradient produced by the main flow is just sufficient to balance the centrifugal force of the boundary layer on the leading part of the blades, and the result is radial equilibrium of the boundary layer. At the rear part of the blade the main flow has zero tangential velocity and thus there is no radial pressure gradient and the boundary-layer flows toward the tip of the blade due to centrifugal force. At intermediate points from leading to trailing edge, the boundary-layer flows more and more toward the tip of the blade. This suggests that where the boundary layer is flowing toward the tip of the blade, the inboard boundary layer must be being thinned out. In the case of the inboard section at design angle of attack the normally thick inboard boundary layer has been thinned sufficiently to make the rotor performance comparable to two-dimensional cascade performance.

At angles of attack greater than design, the air flow entering the rotor has a lower tangential velocity than that of the rotor. At the trailing edge the tangential velocity of the main stream is increased to about 30 percent of the rotor tangential velocity at highest angles of attack. This causes a reduction in the radial pressure gradient over most of the blade and allows greater centrifuging of the boundary layer than at the design condition. Thus at the inboard section for higher angles of attack the boundary layer is thinned more than in the corresponding cascade. The main flow follows the camber line of the blade more closely and, consequently, the turning angle is increased proportionately higher than in cascade for a given increase in angle of attack. For angles of attack lower than design, the inverse is true. The air flow entering the rotor has higher tangential velocities than at design, and the radial pressure gradient is larger in the forward section of the blade passage. At the leading edge, the tangential velocity of the main flow is sufficient to cause the leading-edge boundary layer to flow toward the root of the blade. The result is a reduced net spanwise flow of the boundary layer. For low angles of attack at the inboard section, the boundary layer remains thicker than in the two-dimensional cascade and results in proportionately lower turning angles for the compressor.

The boundary-layer flow was observed by means of small nylon tufts glued to the blades and to the rotor hub between the blades and illuminated with a stroboscopic light. As shown in figure 15(a), the boundary layer on the rotor hub flows from the lower surface of one blade to the upper surface of the preceding blade, that is, from a region of high pressure to one of low pressure. This flow pattern remained unchanged over the angle-of-attack range, except that the tufts in the region just above the trailing edge (marked X) pinwheeled at the highest angles of

attack as though in a stalled turbulent region. The radial flow in the boundary layer on the blade surfaces is indicated by the tufts as shown in figure 15(b). The directions of the tufts as shown are uncorrected for their own centrifugal effect, as the extent to which centrifugal force contributes to the tuft position is unknown. In figure 15(b) the flow was near the design condition. At higher angles of attack the tufts deviated more from the axial direction and at low angles the deviation was less.

Effect of Rotor Wakes on Instrument Accuracy

The survey instrument behind the rotor was in a flow of rapidly varying direction and velocity. As each blade wake passed the survey-instrument wake, it swept over the pressure tubes. The wake was composed of low-velocity air and therefore has a different direction relative to the survey instrument than the main stream. This would result in the survey instrument yawing away from the main stream into the direction of the wakes, and could possibly account for some of the differences between cascade and compressor curves for α against θ shown in figures 11 and 12. It would be desirable to make flow measurements of a rotor without guide vanes (to avoid guide-vane wakes) using a yaw instrument traveling with the rotor to determine the magnitude of this effect.

Since the wake and main stream velocities differ in both magnitude and direction, it appears that they would mix. This is not the case. Although the wake and free stream had different tangential velocities, they do not meet because of the difference in their axial velocities. As this concept has proved confusing to some people, the manner in which the particles travel is now described.

In rotational coordinates, the main stream leaving the rotor and the rotor-blade wakes travel at different speeds in essentially the same direction as shown in figure 16(a). Changing the velocity distribution to stationary coordinates by subtracting the rotational velocity of the rotor results in the distribution shown in figure 16(b). Replacing the stationary velocity distribution with streamlines results in figure 16(c). At first glance figure 16(c) seems to indicate that particles travel across the main stream and abruptly change direction as they flow across the wake. This, however, is not the case. Since figure 16(c) is an instantaneous picture, it can be seen that although particles in the main stream travel along the streamlines, they never enter the wakes, and that particles in the wake remain in the wake. The magnitude of the instrument error that results from these fluctuations in velocity is at the present unknown. Its direction is such as to increase the measured turning angle.

Effect of Guide-Vane Wakes on Instrument Accuracy

The pattern of the data obtained from the instrument behind the rotor indicated that the flow was not uniform in the circumferential direction. The guide vanes seemed to be the most likely cause of this lack of uniformity. To determine the shape and magnitude of the defects produced by the guide-vane wakes behind the rotor, the flow was surveyed using a 16-tube total pressure rake (fig. 5(a)) mounted in place of the usual instrument at station III. Plots of the total-pressure defect for several angles of attack at station III are shown for the outboard, mean, and inboard sections in figures 17(a), 17(b), and 17(c), respectively. Since the instrument was stationary, the shift of the defects shown was due to the increased turning of the air through the rotor with increased angles of attack. In order to obtain accurate data for the determination of θ, an additional instrument was mounted one and one-half guide-vane spaces away in the tangential direction. Thus, one or the other of the instruments was in the uniform stream. It was found that, in general, the total momentum defect of the flow was not appreciably reduced in passing through the rotor as shown in figure 18. In fact, except at the mean section for angles of attack near design, the measured total momentum defect behind the rotor was equal to or larger than the defect measured between the guide vanes and rotor. The greater defect was probably due to the fact that the wake had a much lower dynamic pressure relative to the rotor than the free stream had; yet the static-pressure rise through the rotor was the same for both. If the guide vanes had turned the flow in the conventional direction, the relative dynamic pressure of the wake would be nearly equal to that of the free stream.

Normal-Force Coefficients

As a check on the accuracy of the pressure distributions, the normal-force coefficients were computed from the compressor data by three methods: (1) from integration of measured pressure distributions $(c_n)_P$, (2) from measured change in momentum and static pressure when the drag force was neglected $(c_n)_M$, and (3) from ideal change in momentum and static pressure when corrected values of α and θ were used $(c_n)_\theta$. Plots of these coefficients are shown in figure 19. The values of section normal-force coefficient computed from the pressure distribution $(c_n)_P$ differ from those computed from momentum change $(c_n)_M$ primarily because of experimental inaccuracies and radial flow. The value of $(c_n)_\theta$ will ordinarily be higher since it represents an ideal condition. In general, $(c_n)_P$ and $(c_n)_M$ are in good agreement; this fact indicates that radial flow and profile drag have a small effect. The values of $(c_n)_P$ and $(c_n)_M$ are in progressively worse agreement with $(c_n)_\theta$ as θ is increased, primarily because the ideal theoretical static-pressure rise was not realized. The measured static-pressure rise was used in

computing $(c_n)_M$ and the ideal in computing $(c_n)_\theta$. The difference between the measured and the ideal pressure rise was greatest at highest angles of attack where the large radial flow of the boundary layer produced high turning angles that were used in computing the values of $(c_n)_\theta$.

CONCLUSIONS

The turning angles, pressure rise, and pressure distribution about the blades of a rotor having 65-series compressor blades were measured and compared with similar data for the same blade profiles measured in a two-dimensional porous-wall cascade tunnel. Guide vanes, necessary to produce a free-vortex flow ahead of the rotor, produced secondary disturbances not present in the cascade. The secondary effects are considered small enough to permit a direct comparison of rotor and cascade data. From an examination of the data, it is found that:

1. The two-dimensional cascade-tunnel data agreed closely with the rotor data at the design conditions of the rotor.

2. At off-design angles of attack, differences were observed in performance; secondary flows have a large effect on the operating characteristics of the rotor. This result was found especially true near the inner casing. The deviations in performance were attributed to radial flow of the blade-surface boundary layer due to centrifugal force being out of balance with the radial static-pressure gradient.

3. The total-pressure defects produced by the upstream row of stator blades were not significantly dispersed by the rotor, but rather the integrated total-pressure defect was greater after passing through the rotor.

4. The ratio between the local velocity and the entering velocity remains nearly constant at one point on the convex surface of NACA 65-series compressor blades. If this phenomenon exists at high speeds, it may be used to determine impact and static pressures in a multistage axial-flow compressor by orifices located at the desired radial stations at the proper chordwise position of the stator blades and pitot tubes.

Langley Aeronautical Laboratory,
National Advisory Committee for Aeronautics,
Langley Field, Va., September 25, 1951.

REFERENCES

1. Weske, John R.: An Investigation of the Aerodynamic Characteristics of a Rotating Axial-Flow Blade Grid. NACA TN 1128, 1947.

2. Mühlemann, Ernst: Experimentelle Untersuchungen an einer axialen Gebläsestufe. Mitt. Nr. 12, Inst. für Aerod. Tech. H. S. Zurich, Gebr. Leemann & Co. (Zürich), 1946.

3. Erwin, John R., and Emery, James C.: Effect of Tunnel Configuration and Testing Technique on Cascade Performance. NACA Rep. 1016, 1951. (Supersedes NACA TN 2028.)

4. Herrig, L. Joseph, Emery, James C., and Erwin, John R.: Systematic Two-Dimensional Cascade Tests of NACA 65-Series Compressor Blades at Low Speeds. NACA RM L51G31, 1951.

5. Runckel, Jack F., and Davey, Richard S.: Pressure-Distribution Measurements on the Rotating Blades of a Single-Stage Axial-Flow Compressor. NACA TN 1189, 1947.

6. Katzoff, S., and Hannah, Margery E.: Further Comparisons of Theoretical and Experimental Lift and Pressure Distributions on Airfoils in Cascade at Low-Subsonic Speed. NACA TN 2391, 1951.

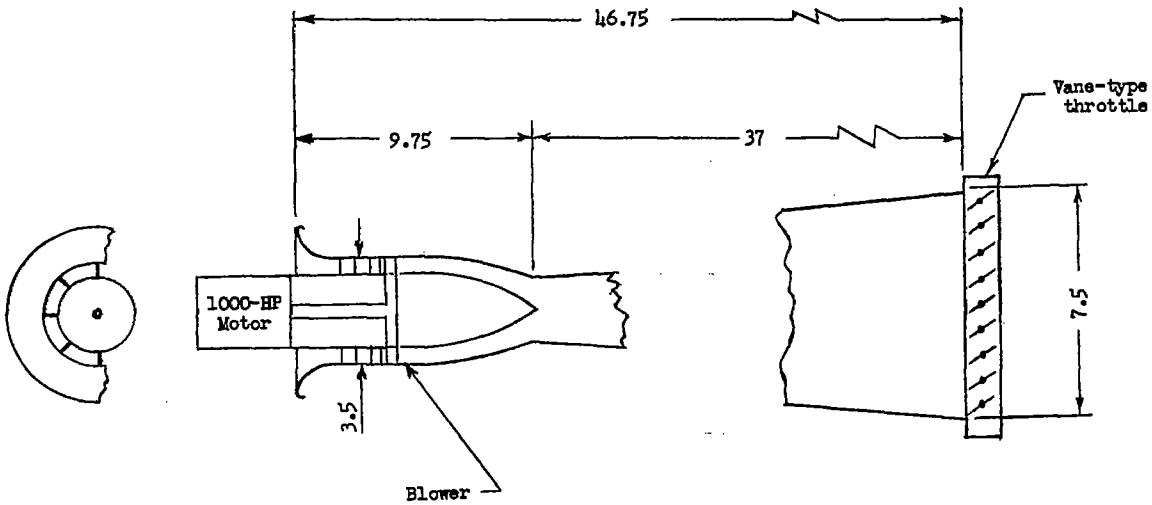

(a) Schematic sketch of compressor test arrangement. (All linear dimensions are in feet.)

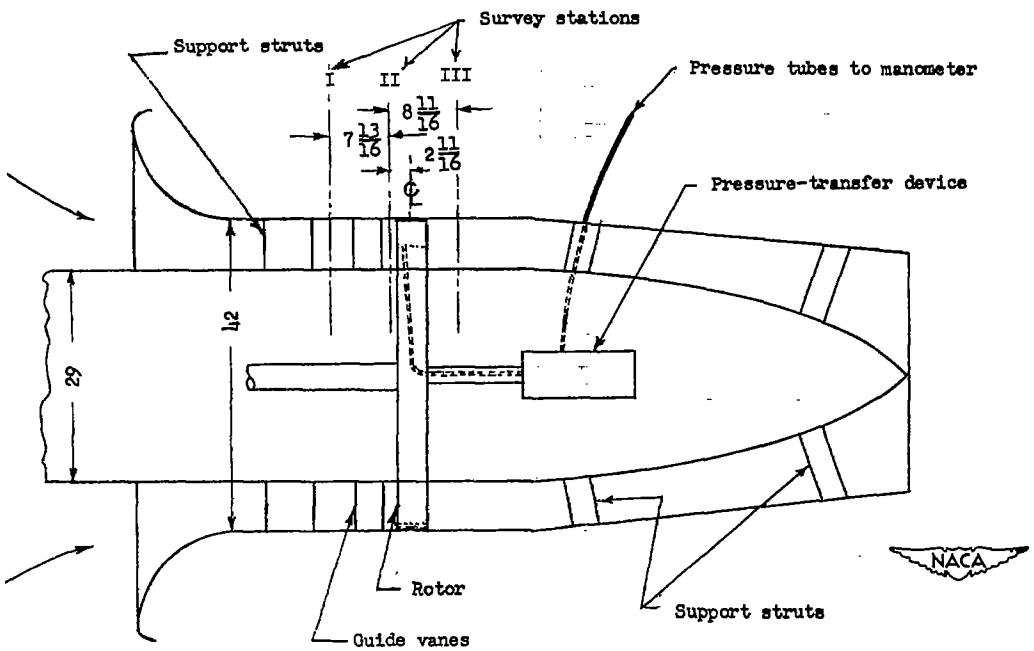

(b) Schematic sketch of test section. (All linear dimensions are in inches.)

Figure 1.- General arrangement.

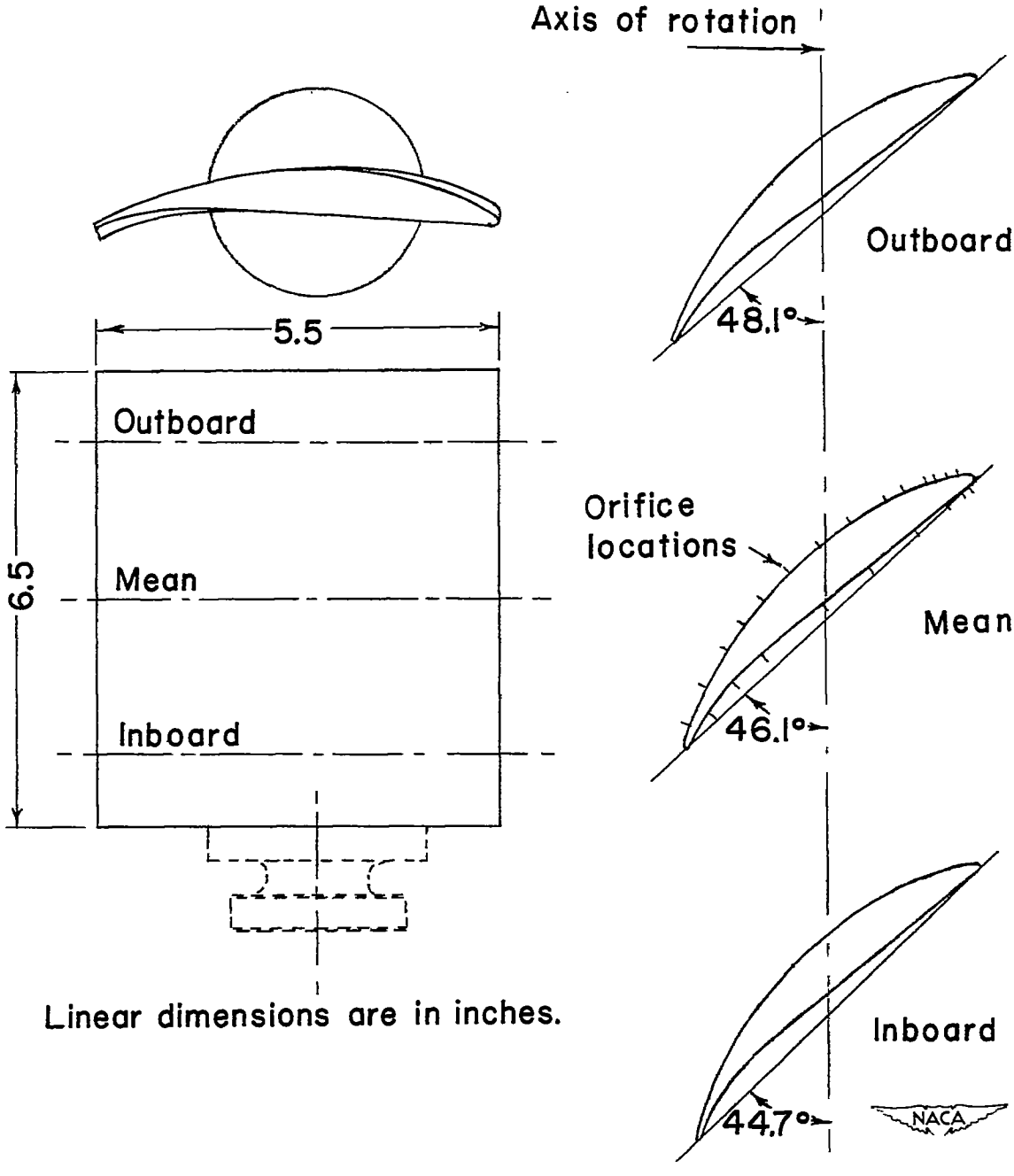

Figure 2.- Sketch of rotor blades.

	ψ_{II}, deg	β, deg	α, deg	θ, deg
Outboard	36.4	60	11.9	15.1
Mean	41.1	59.7	13.6	19.7
Inboard	46.9	60.2	15.5	25.6

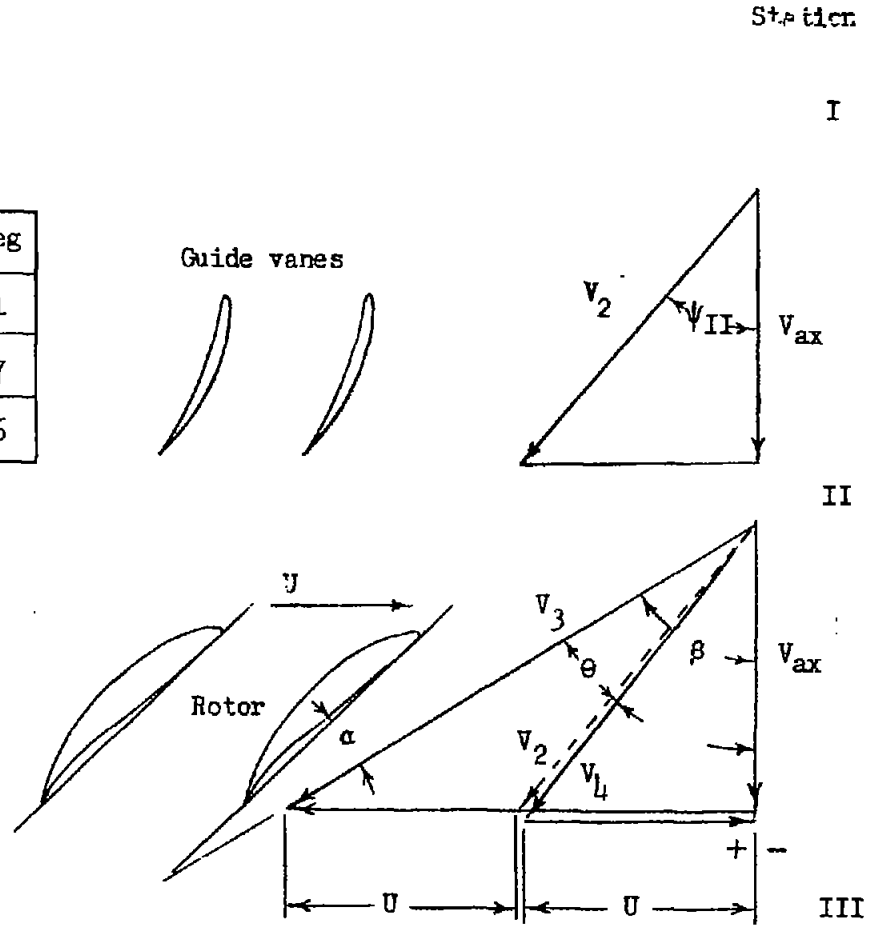

Figure 3.- Velocity diagram at design conditions.

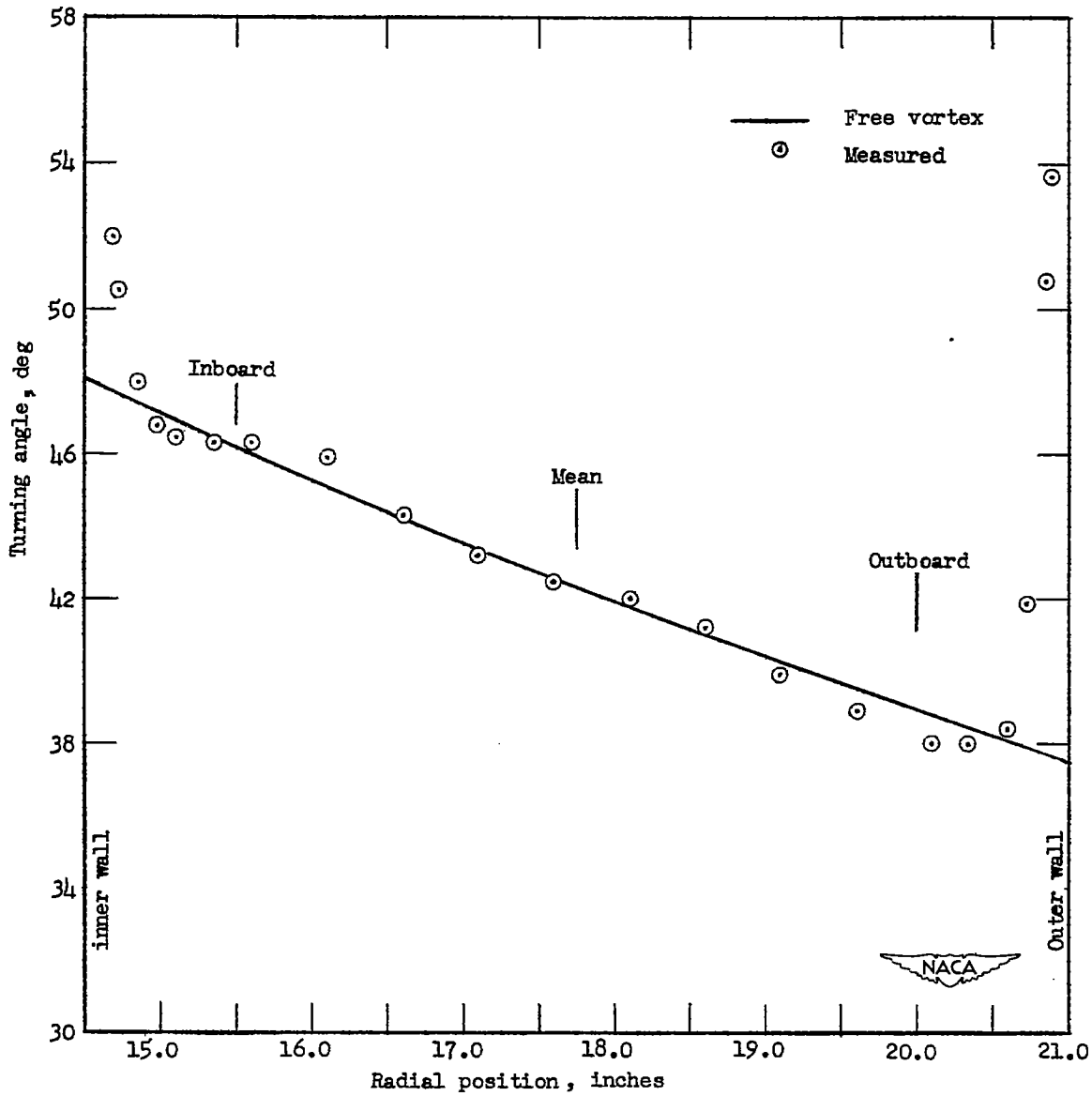

Figure 4.- Comparison of measured guide-vane turning angle with angles required for free-vortex flow.

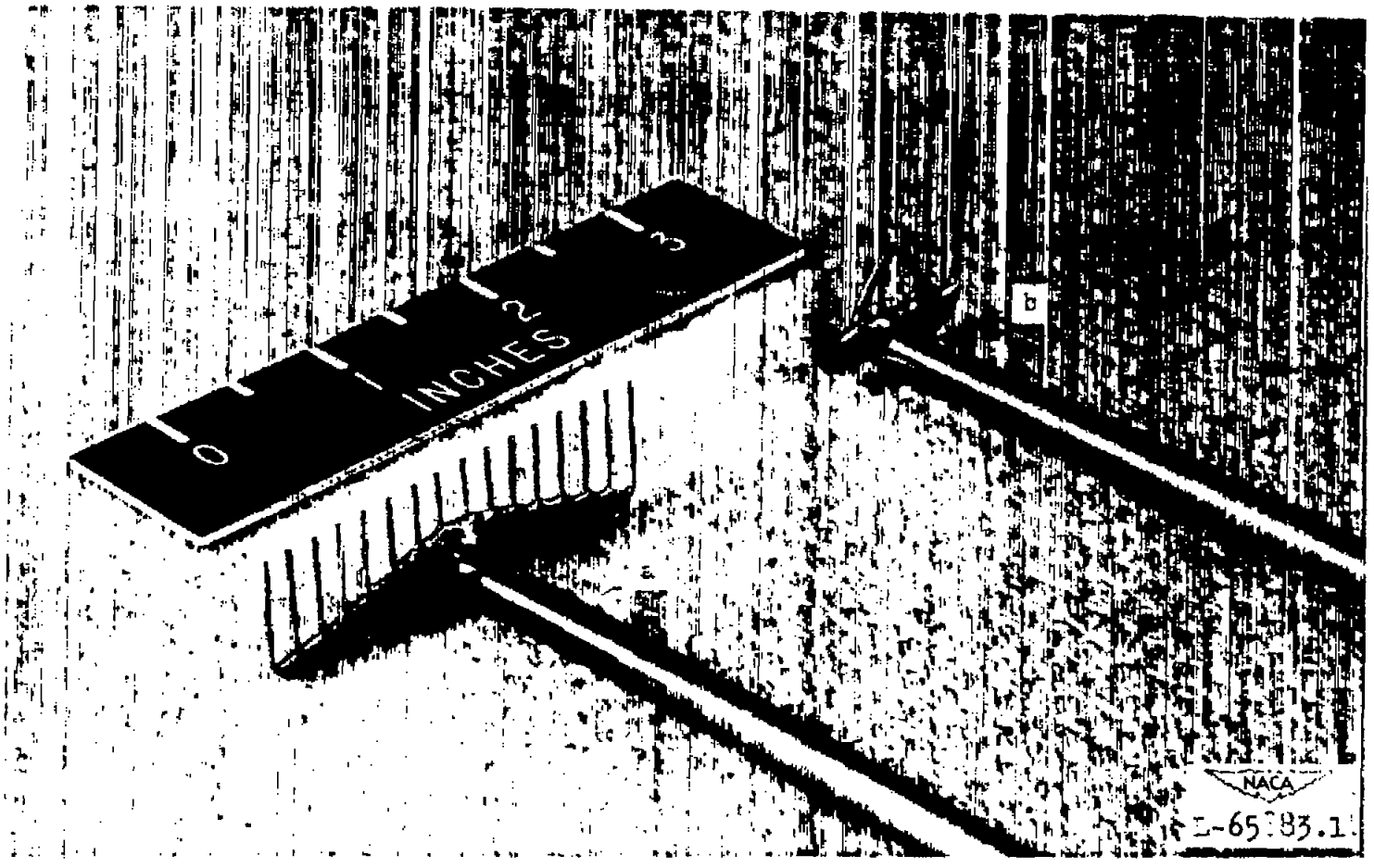

(a) Total head rake.

(b) Total head, yaw claw, and static-tube instrument.

Figure 5.- Survey instruments.

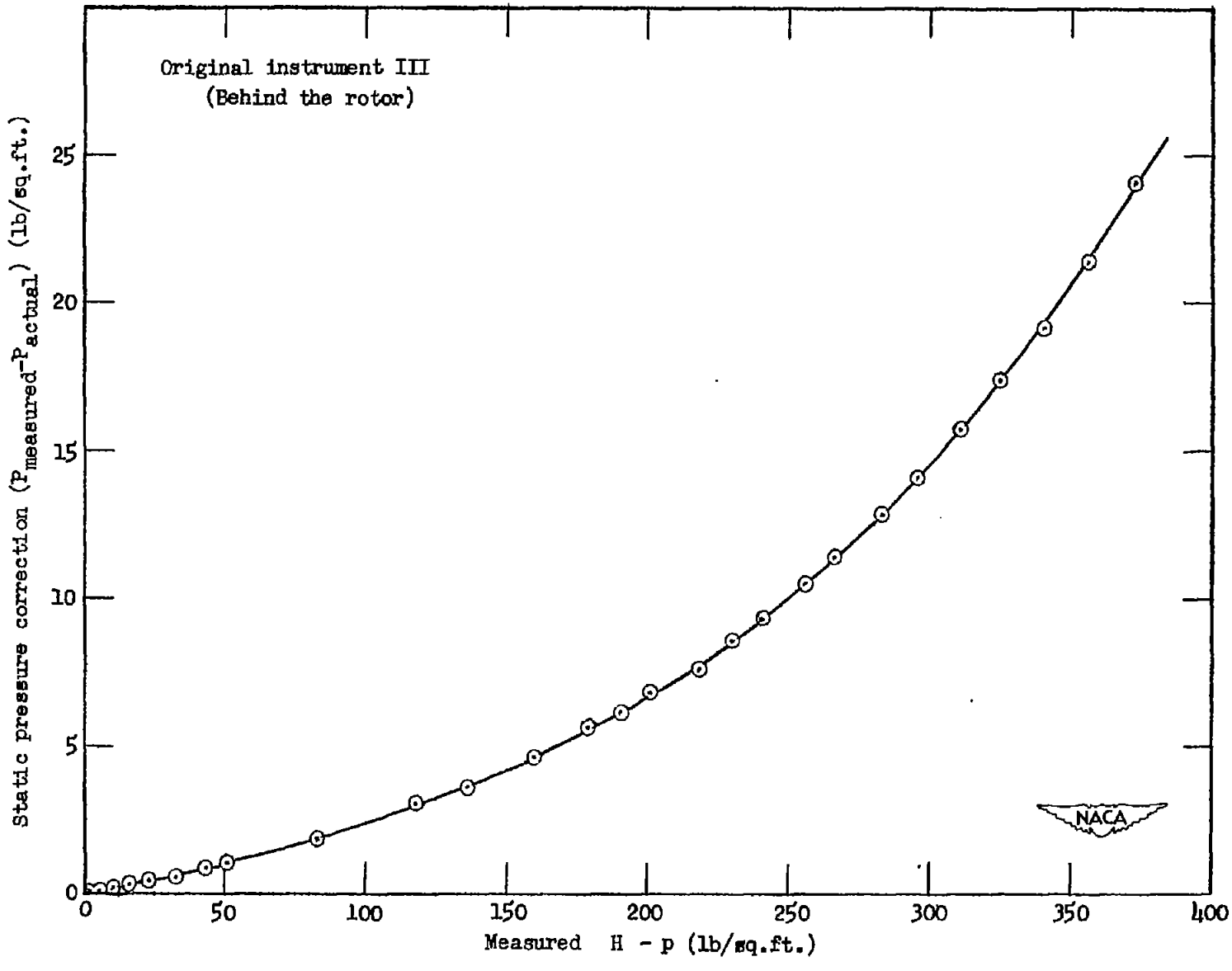

Figure 6.- A typical calibration curve.

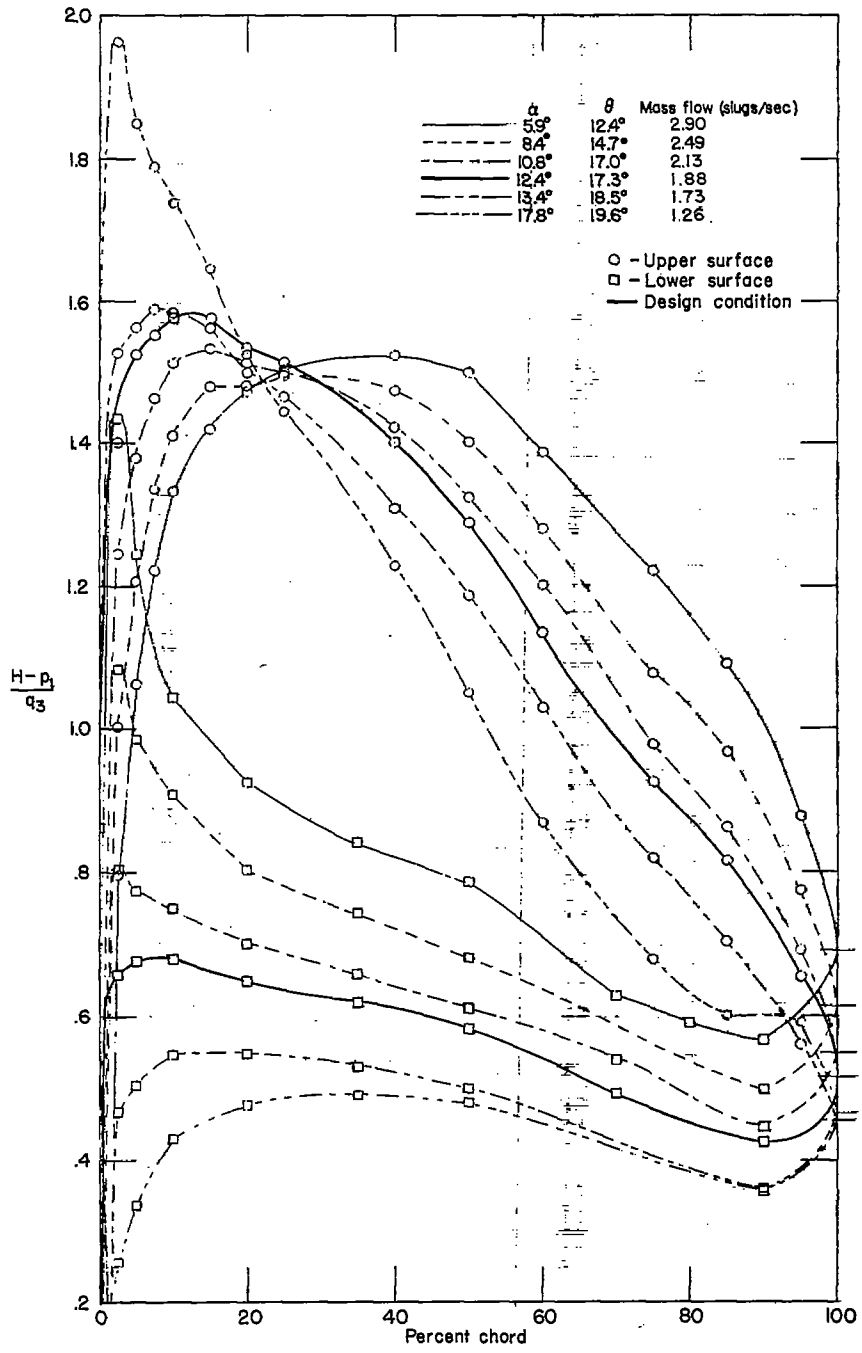

(a) Outboard section.

Figure 7.- Pressure distributions at various angles of attack.

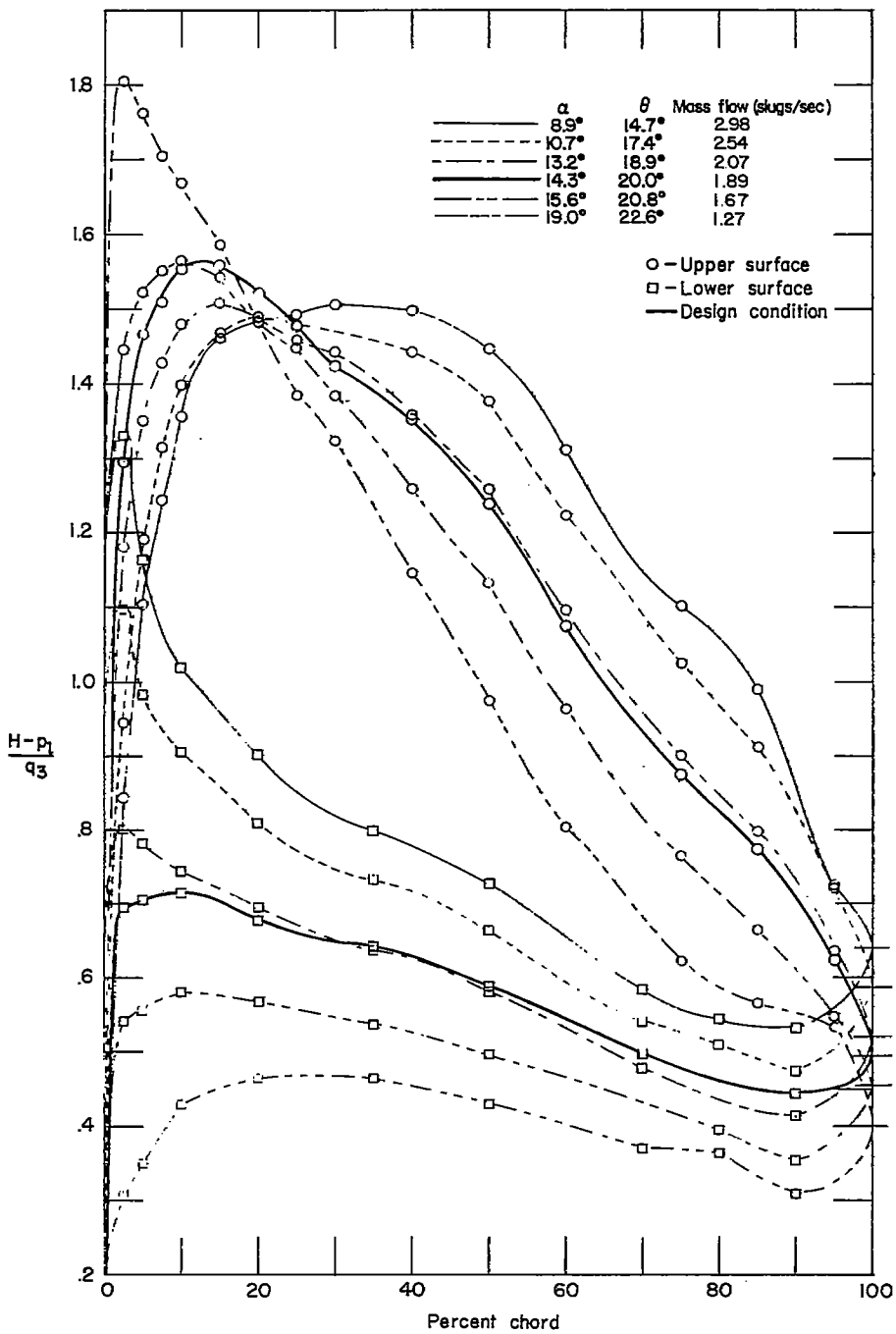

(b) Mean section.

Figure 7.- Continued.

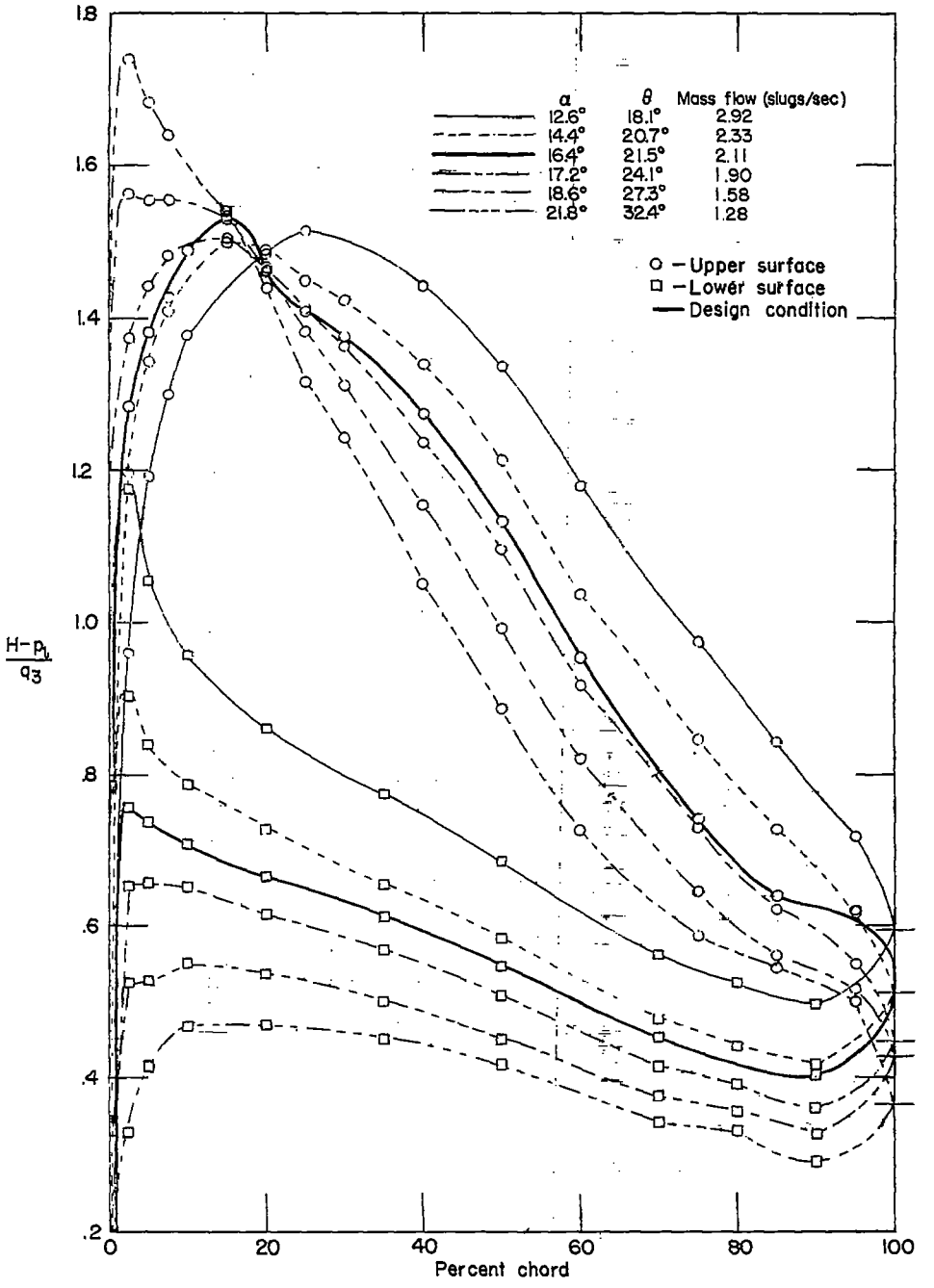

(c) Inboard section.

Figure 7.- Concluded.

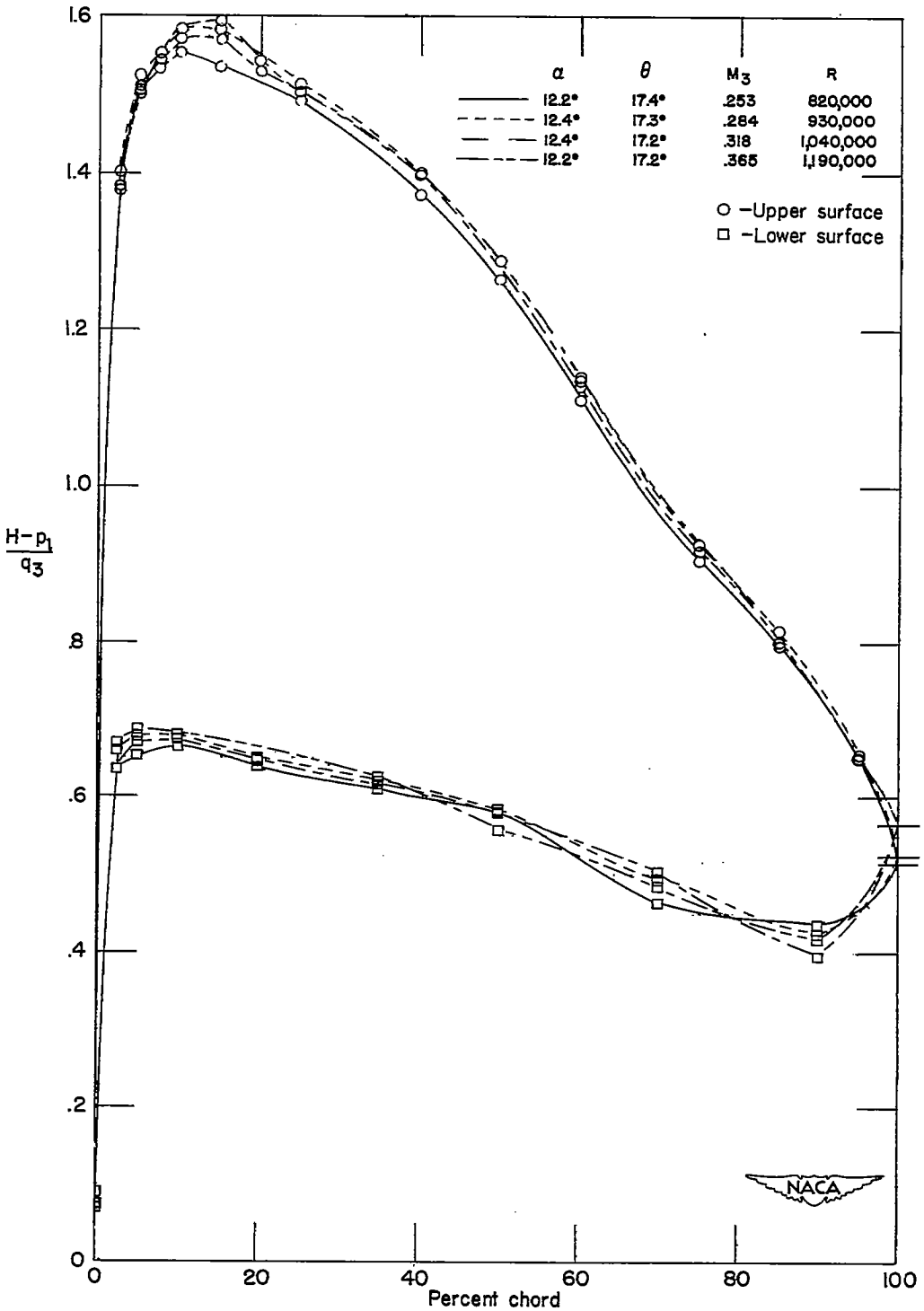

(a) Outboard section.

Figure 8.- Pressure distributions at design angle of attack, with M_3 variation.

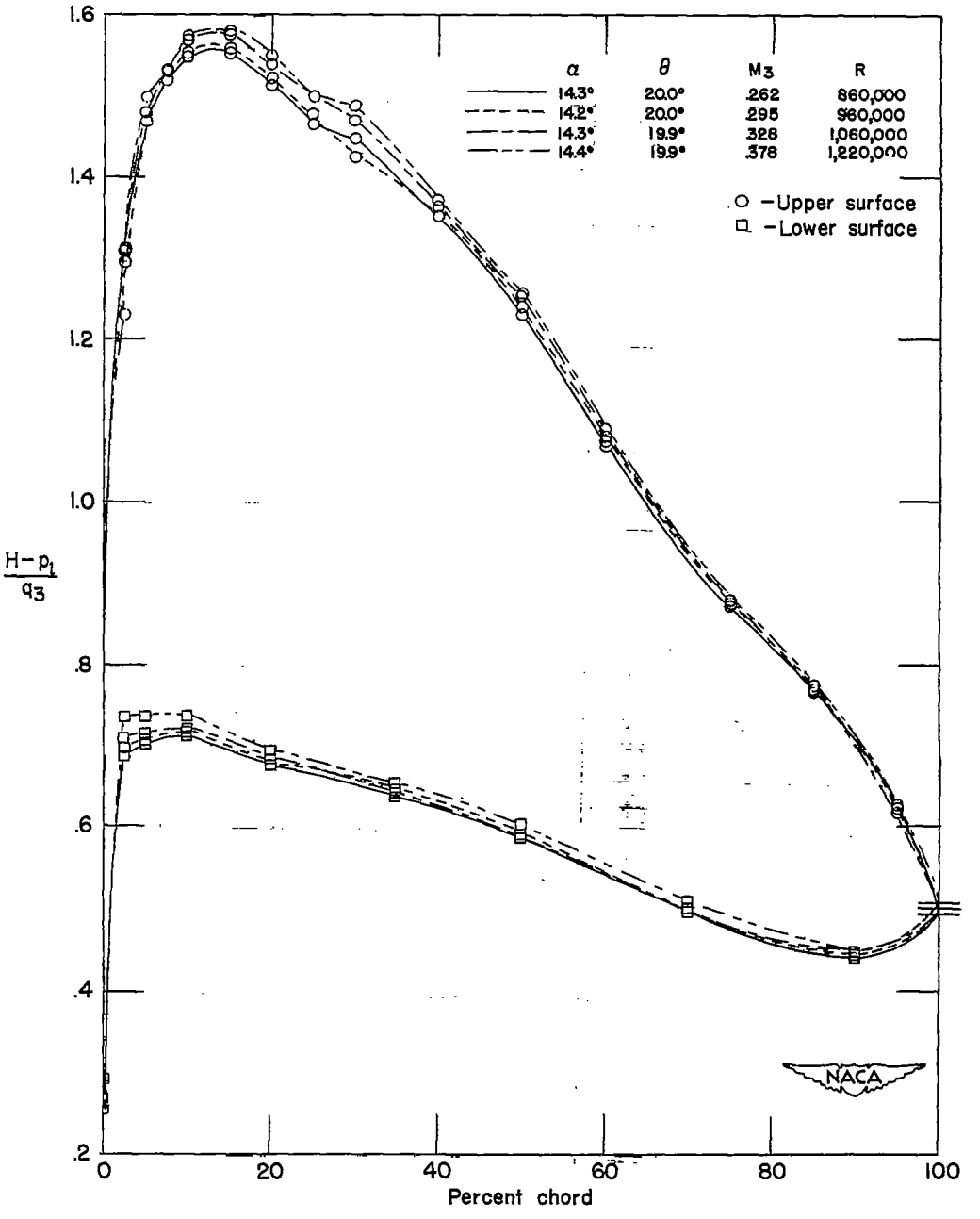

(b) Mean section.

Figure 8.- Continued.

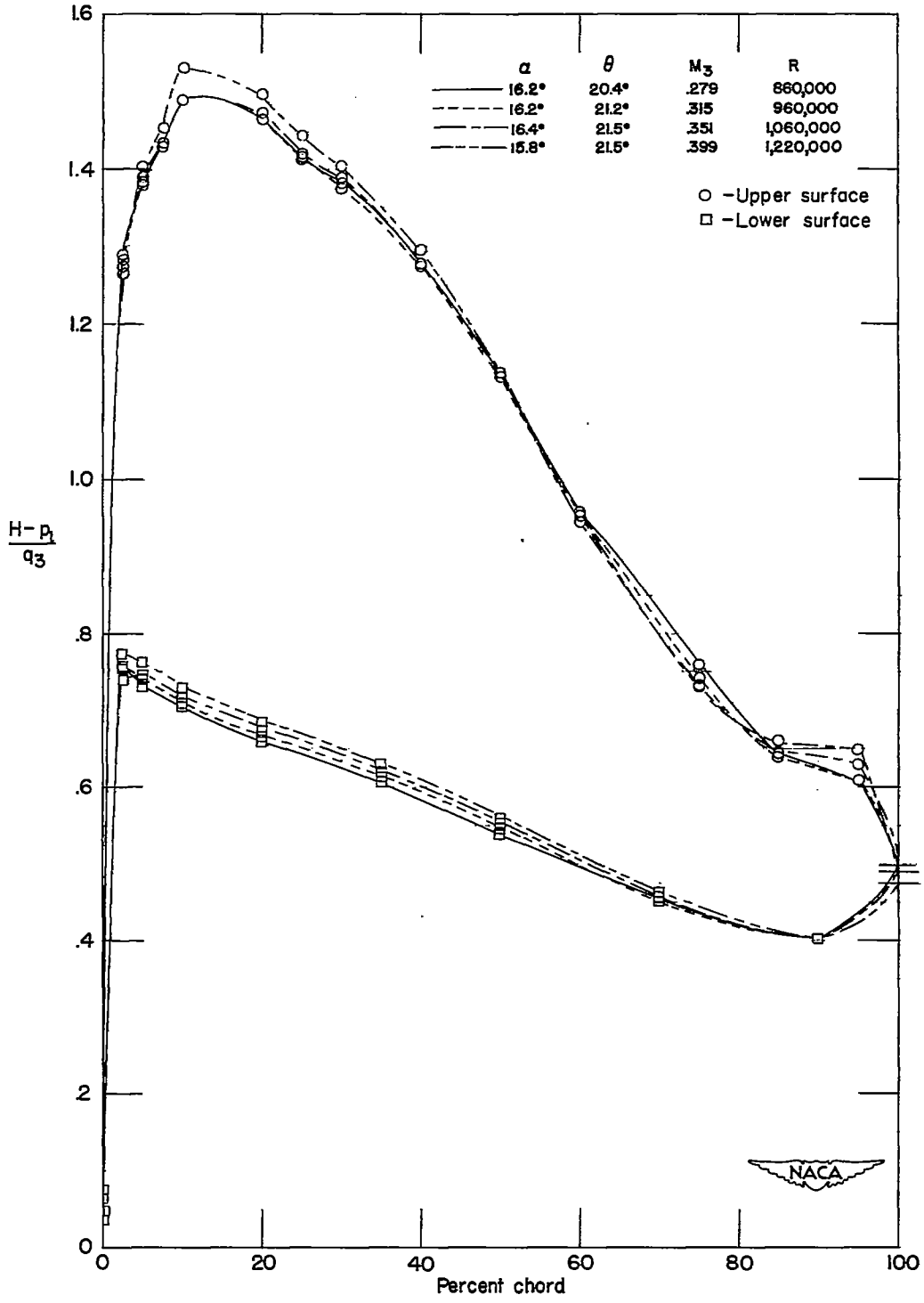

(c) Inboard section.

Figure 8.- Concluded.

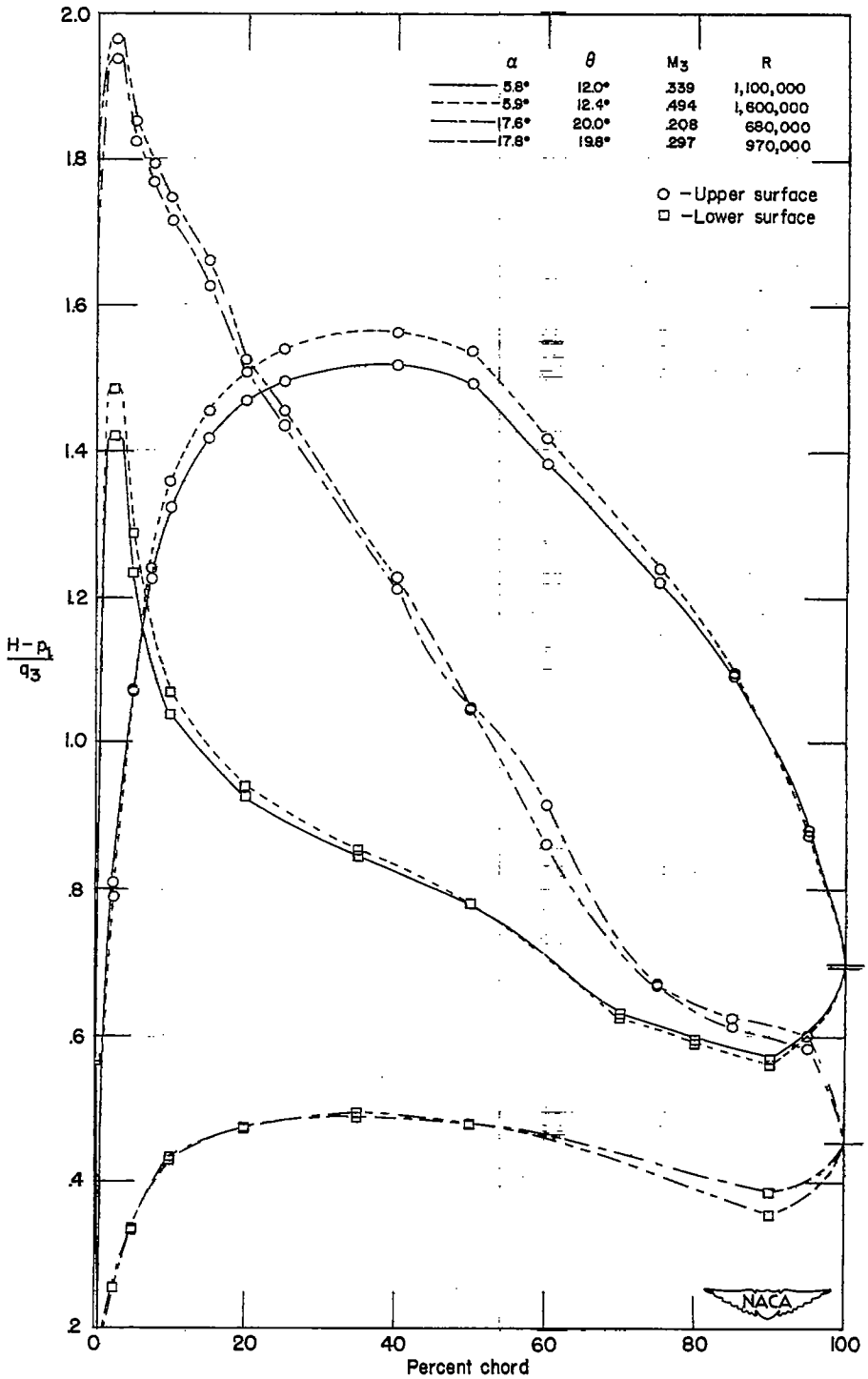

(a) Outboard section.

Figure 9.- Pressure distributions at highest and lowest angles of attack.

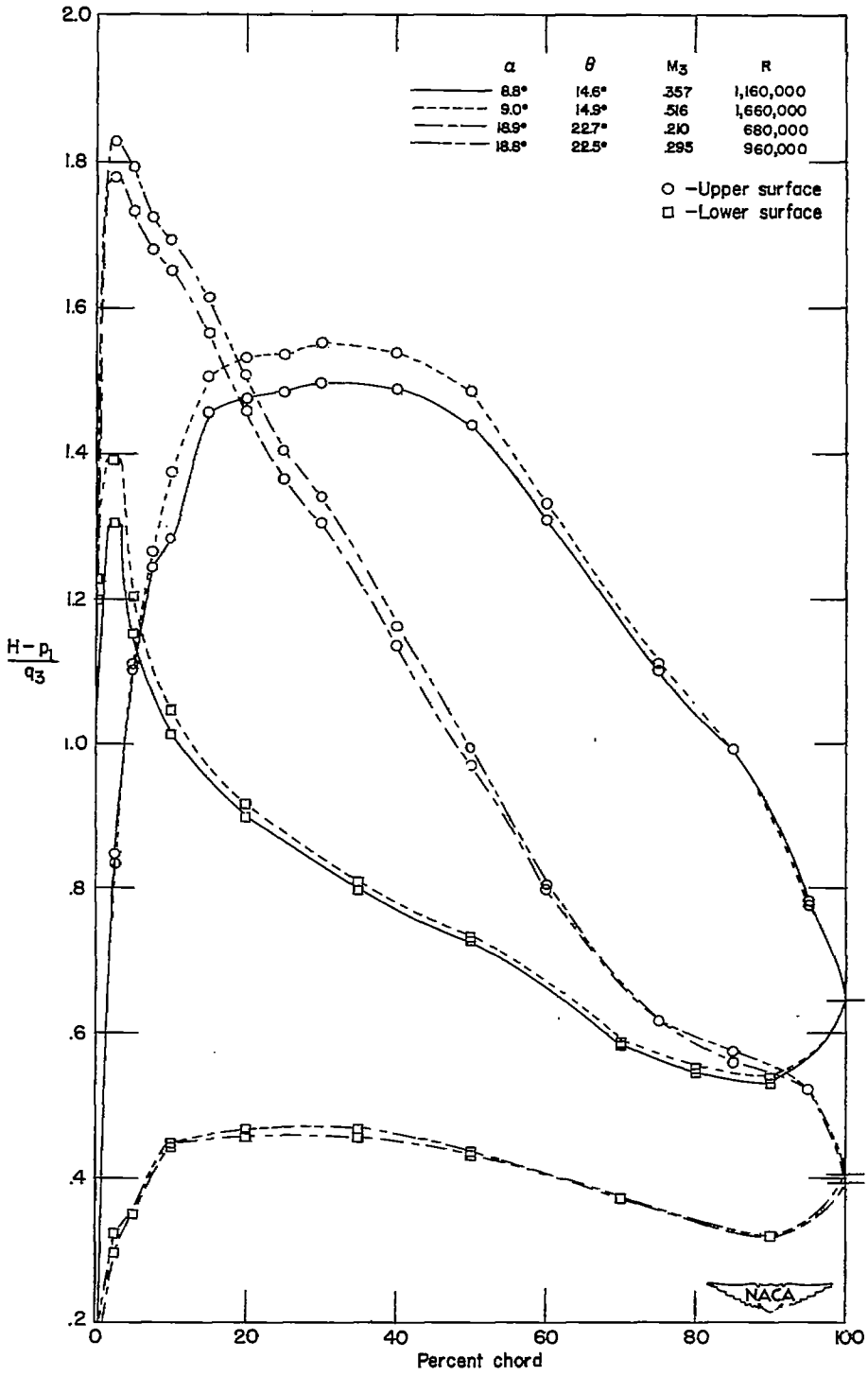

(b) Mean section.

Figure 9.- Continued.

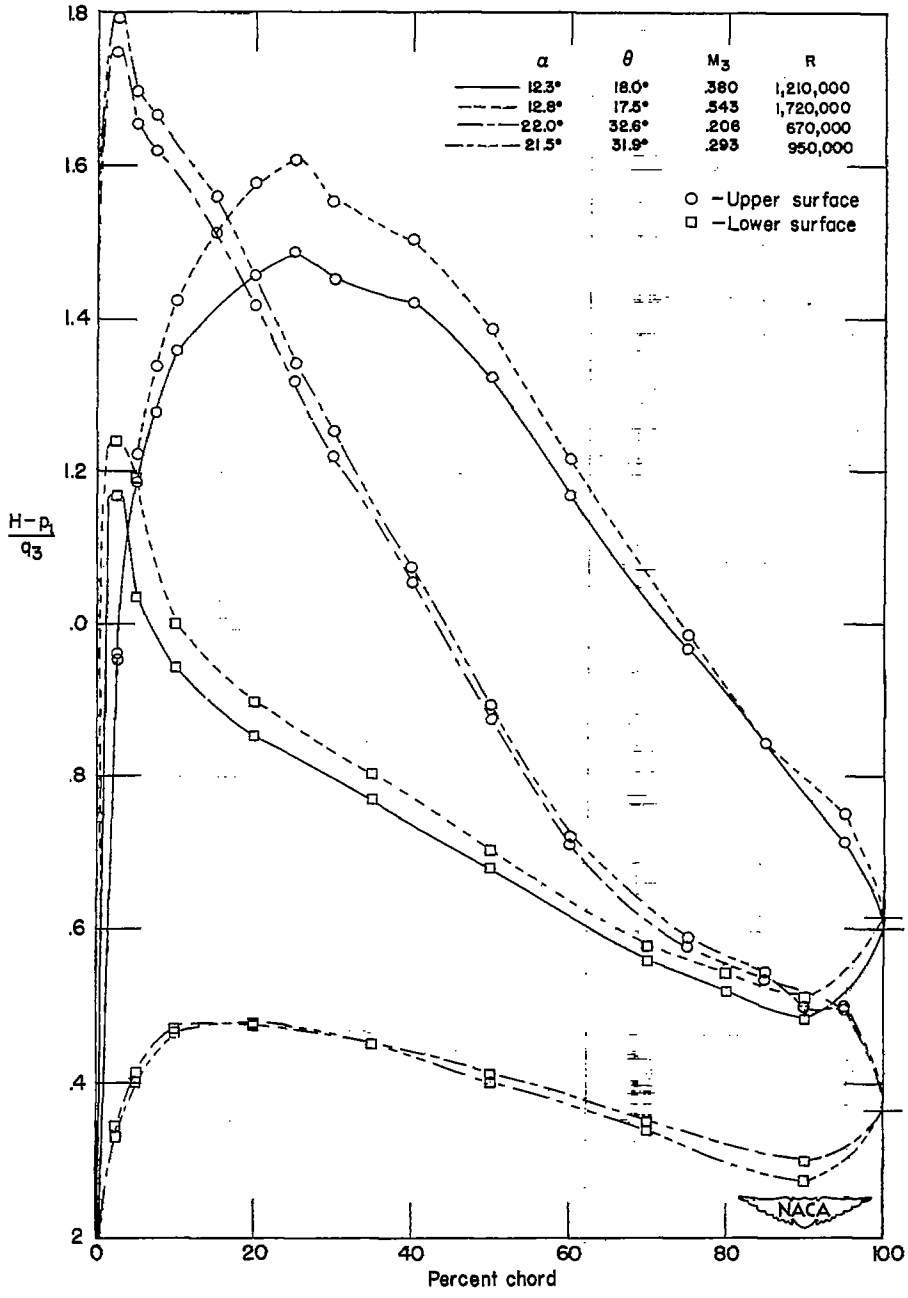

(c) Inboard section.

Figure 9.- Concluded.

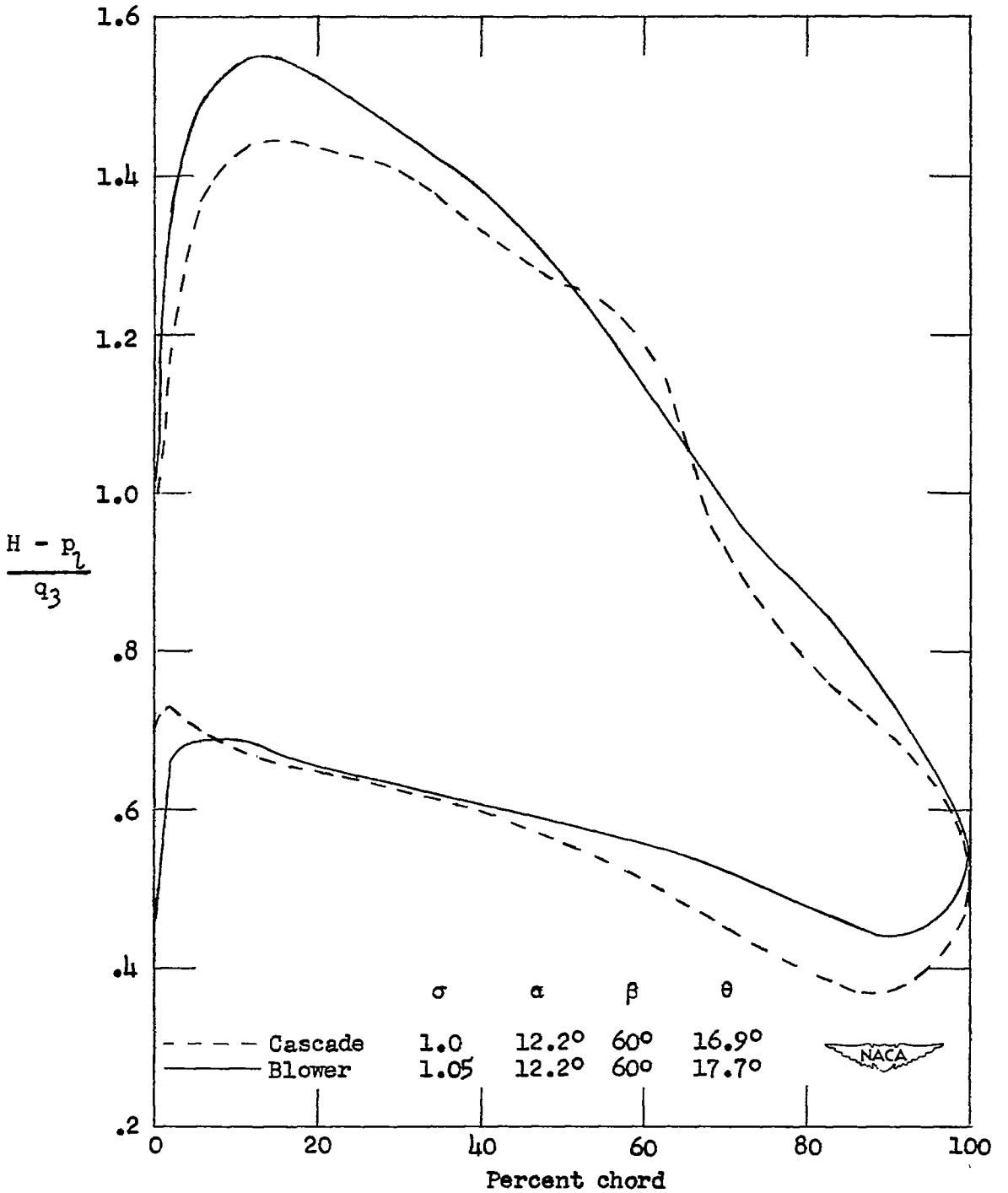

(a) 65-(10.96)10 (outboard section).

Figure 10.- Comparison of blower and cascade pressure distributions at design angle of attack.

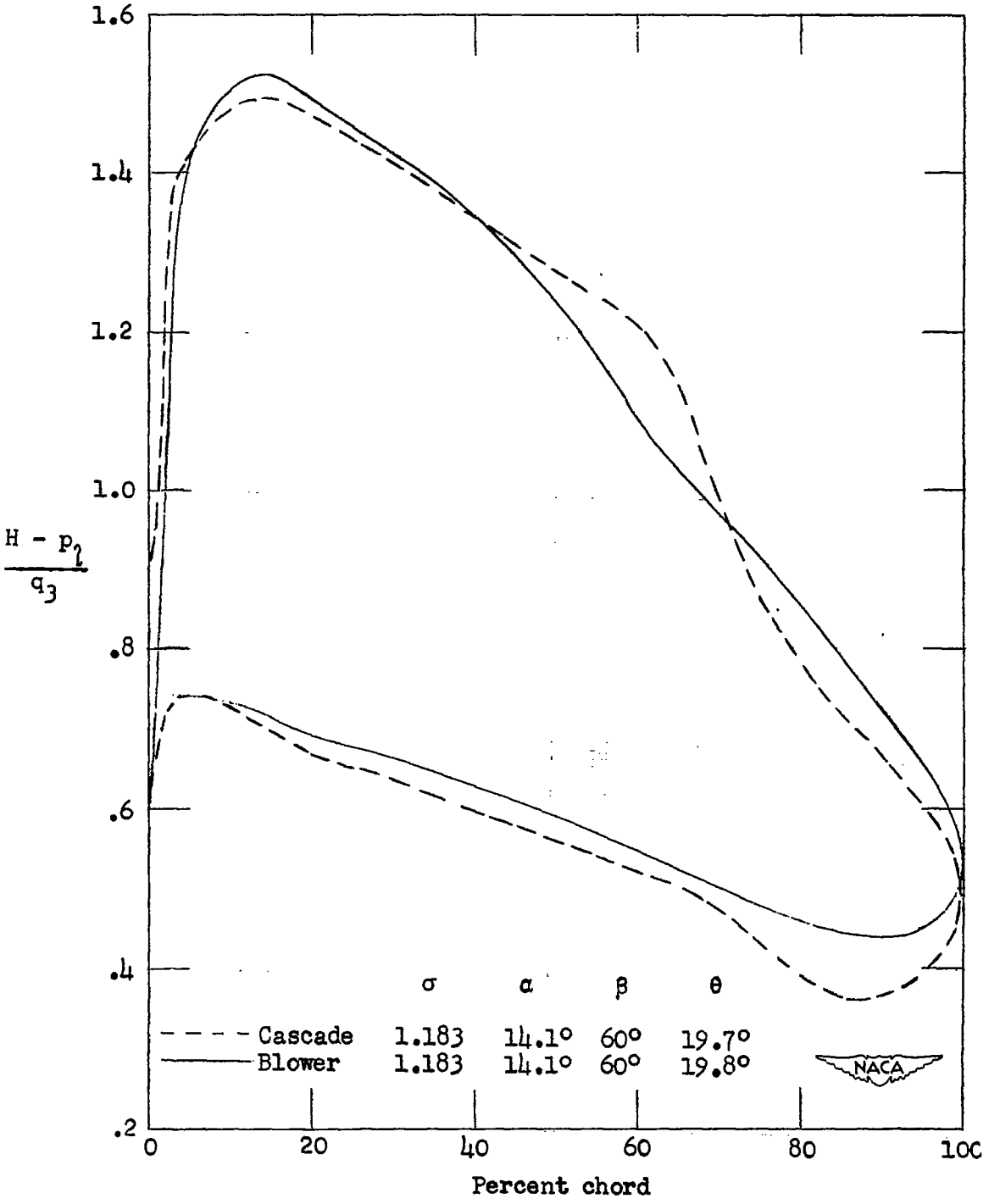

(b) 65-(12)10 (mean section).

Figure 10.- Continued.

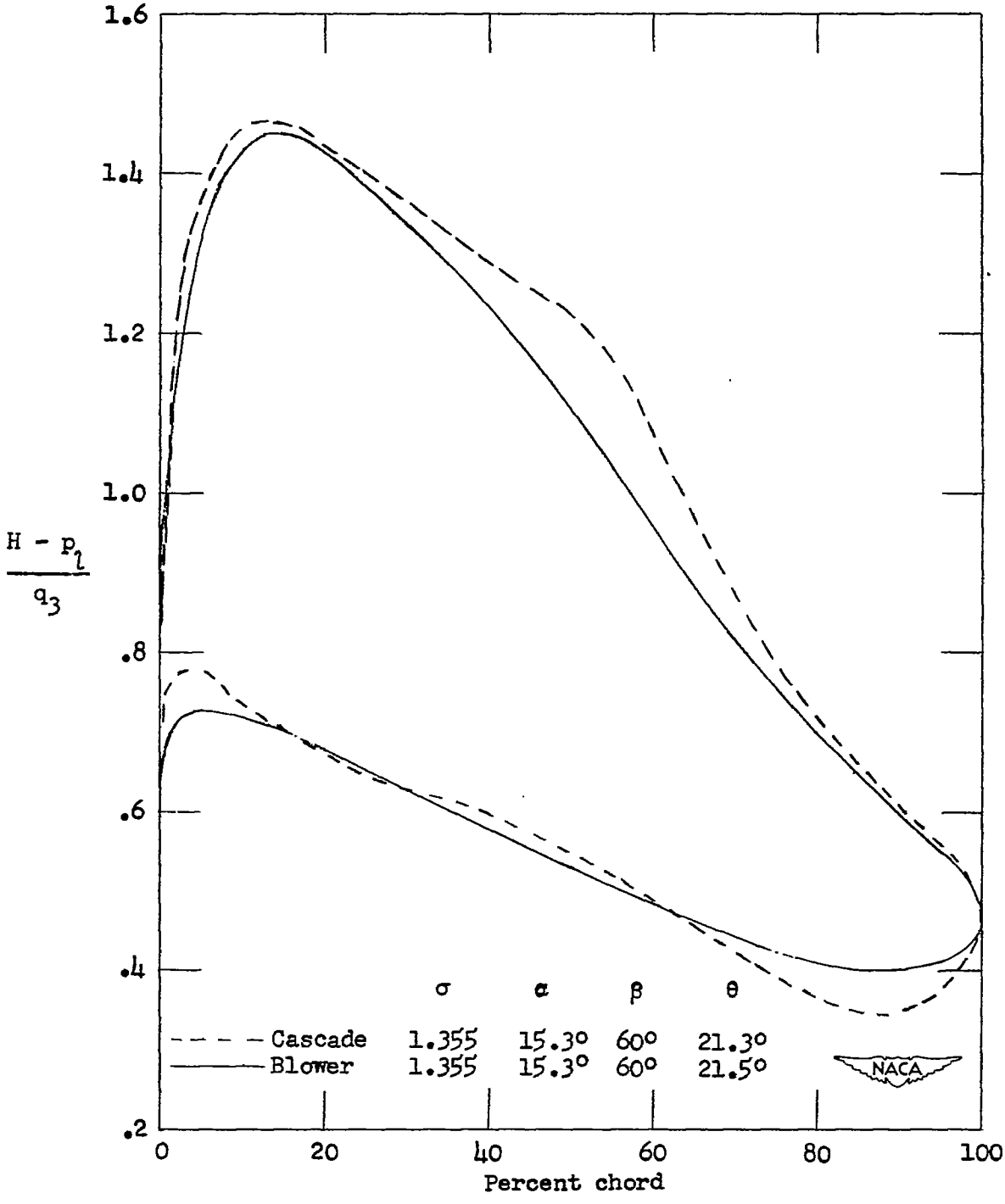

(c) 65-(13.04)10 (inboard section).

Figure 10.- Concluded.

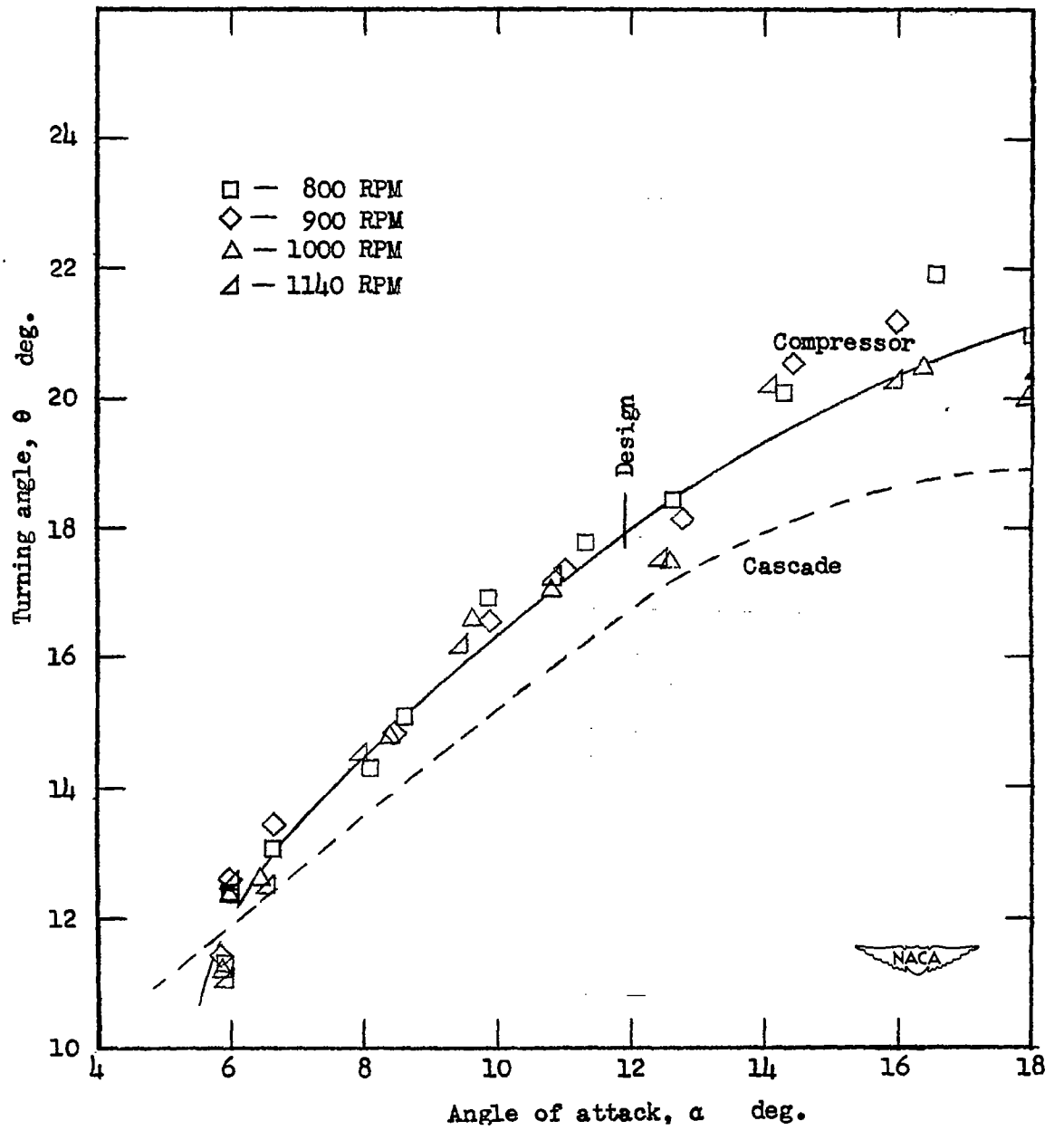

(a) At the outboard section.

Figure 11.- Turning angle against angle of attack.

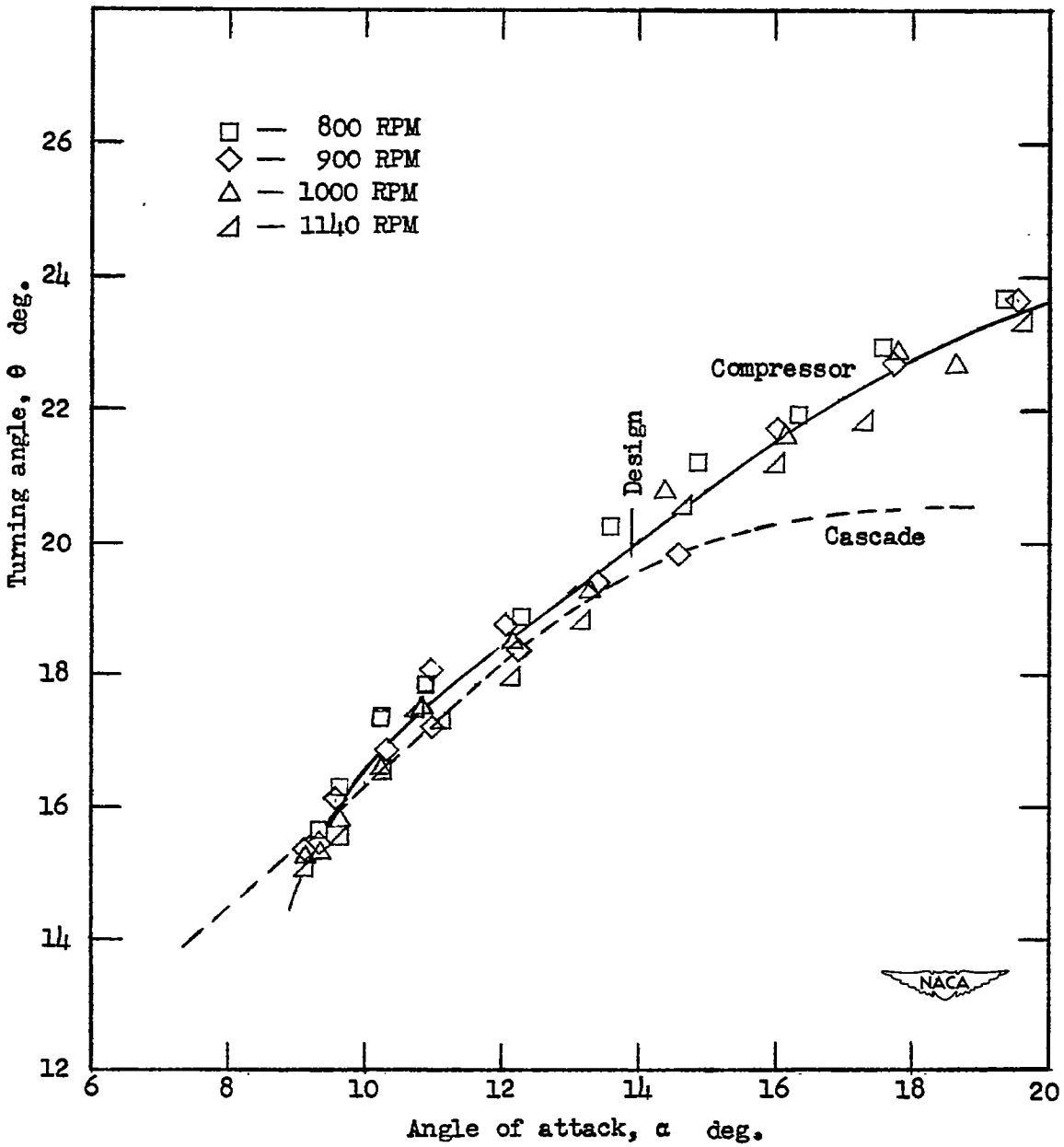

(b) At the mean section.

Figure 11.- Continued.

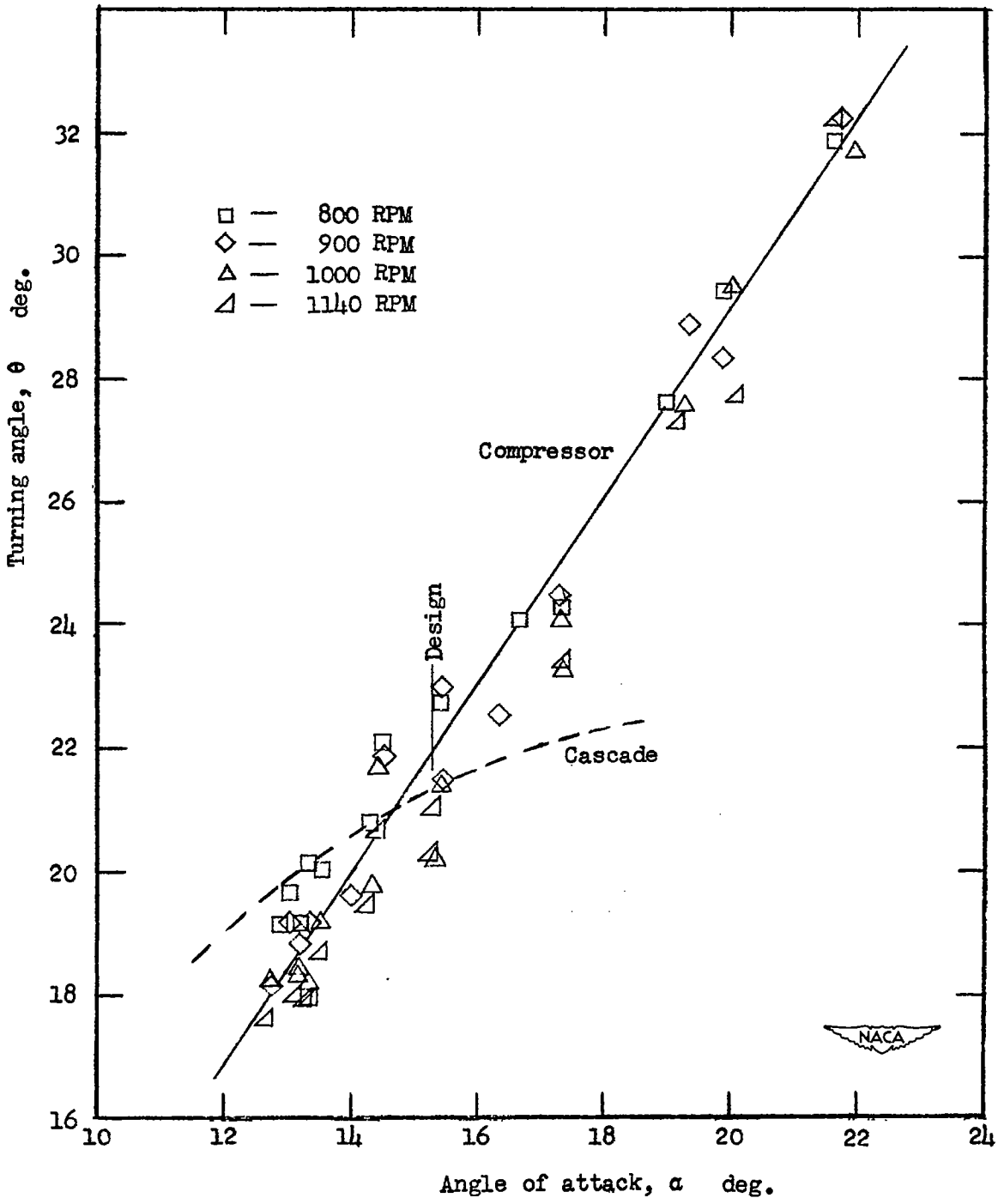

(c) At the inboard section.

Figure 11.- Concluded.

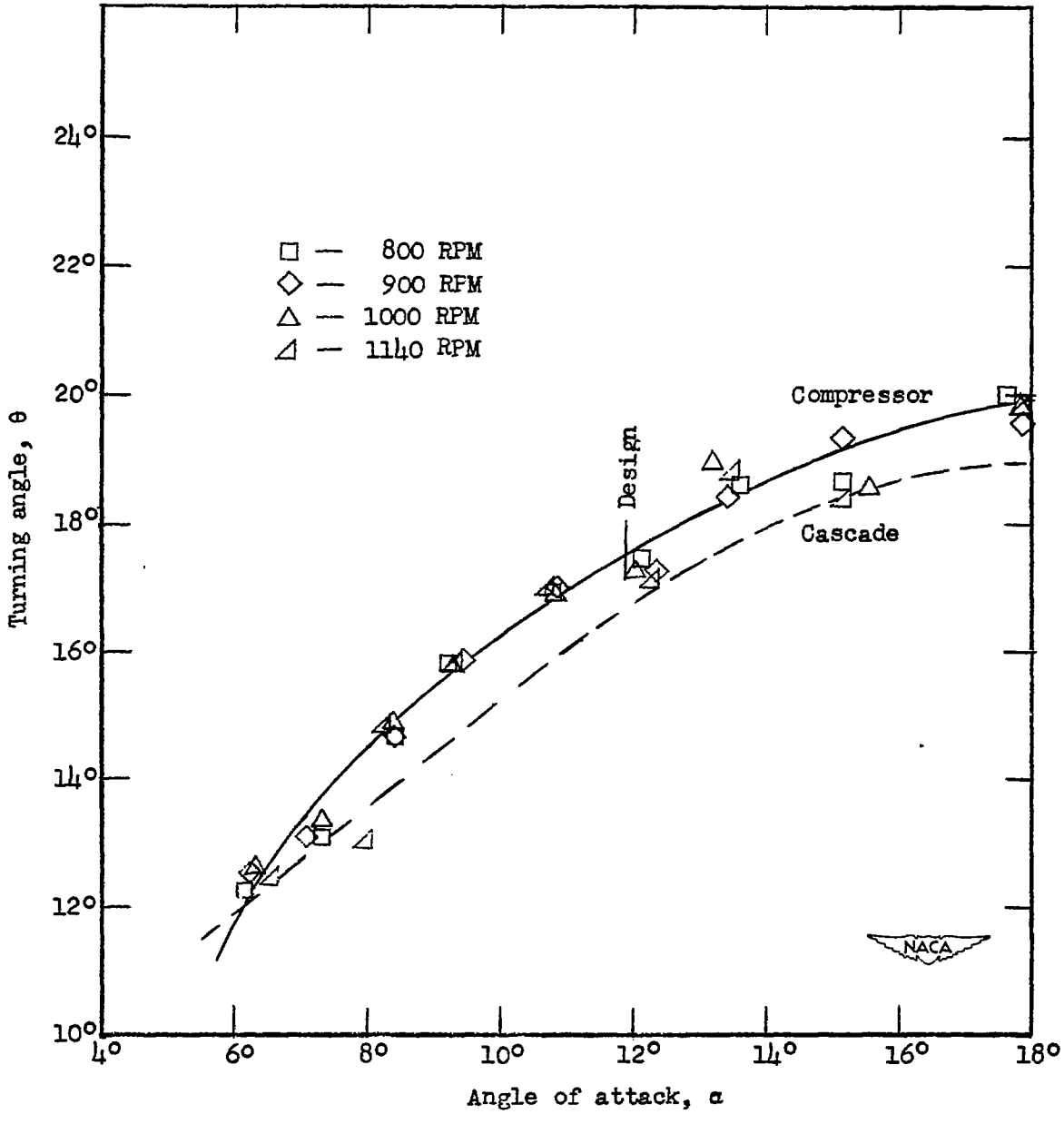

(a) At the outboard section.

Figure 12.- Turning angle against angle of attack, corrected to a mean axial velocity.

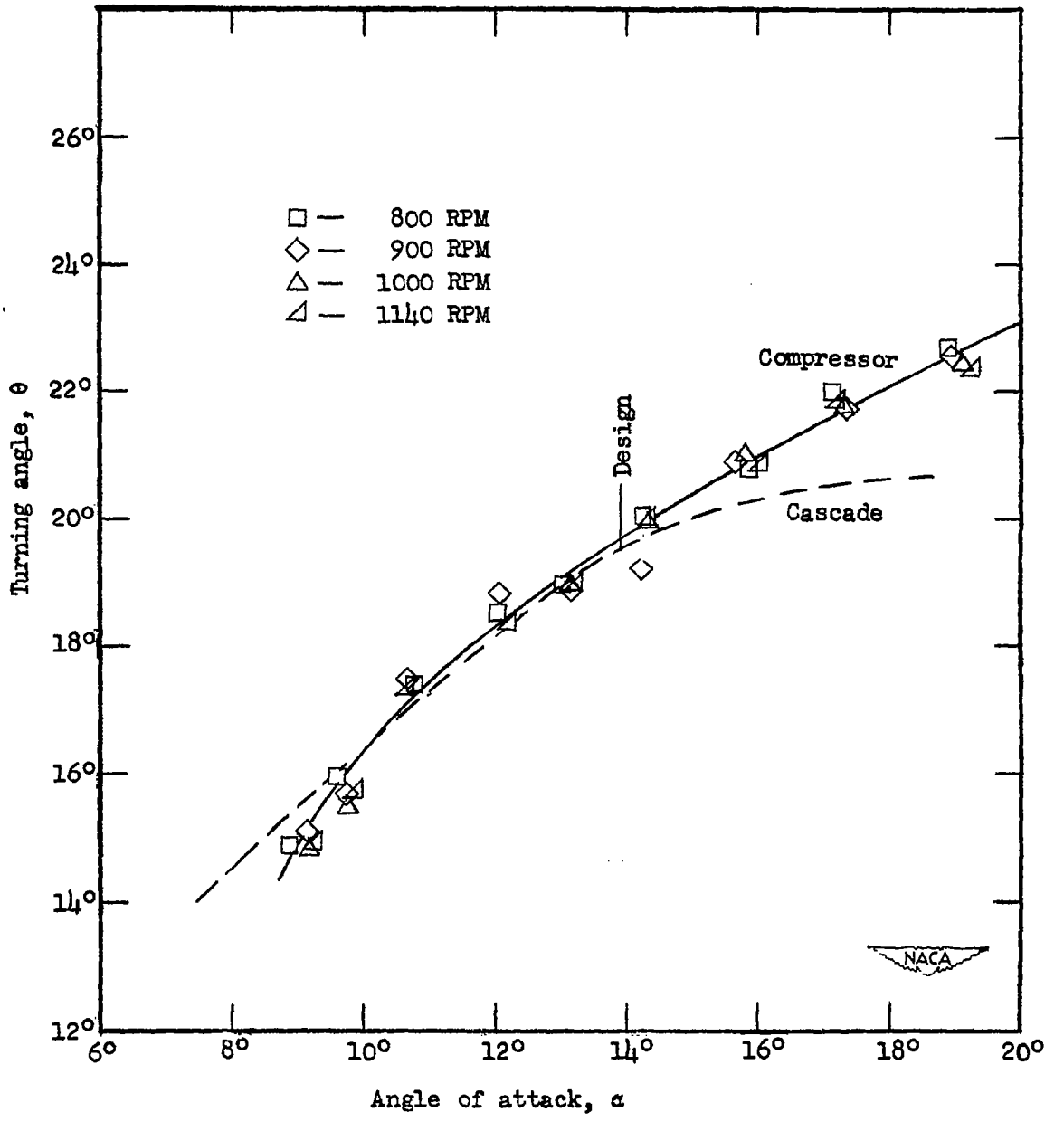

(b) At the mean section.

Figure 12.- Continued.

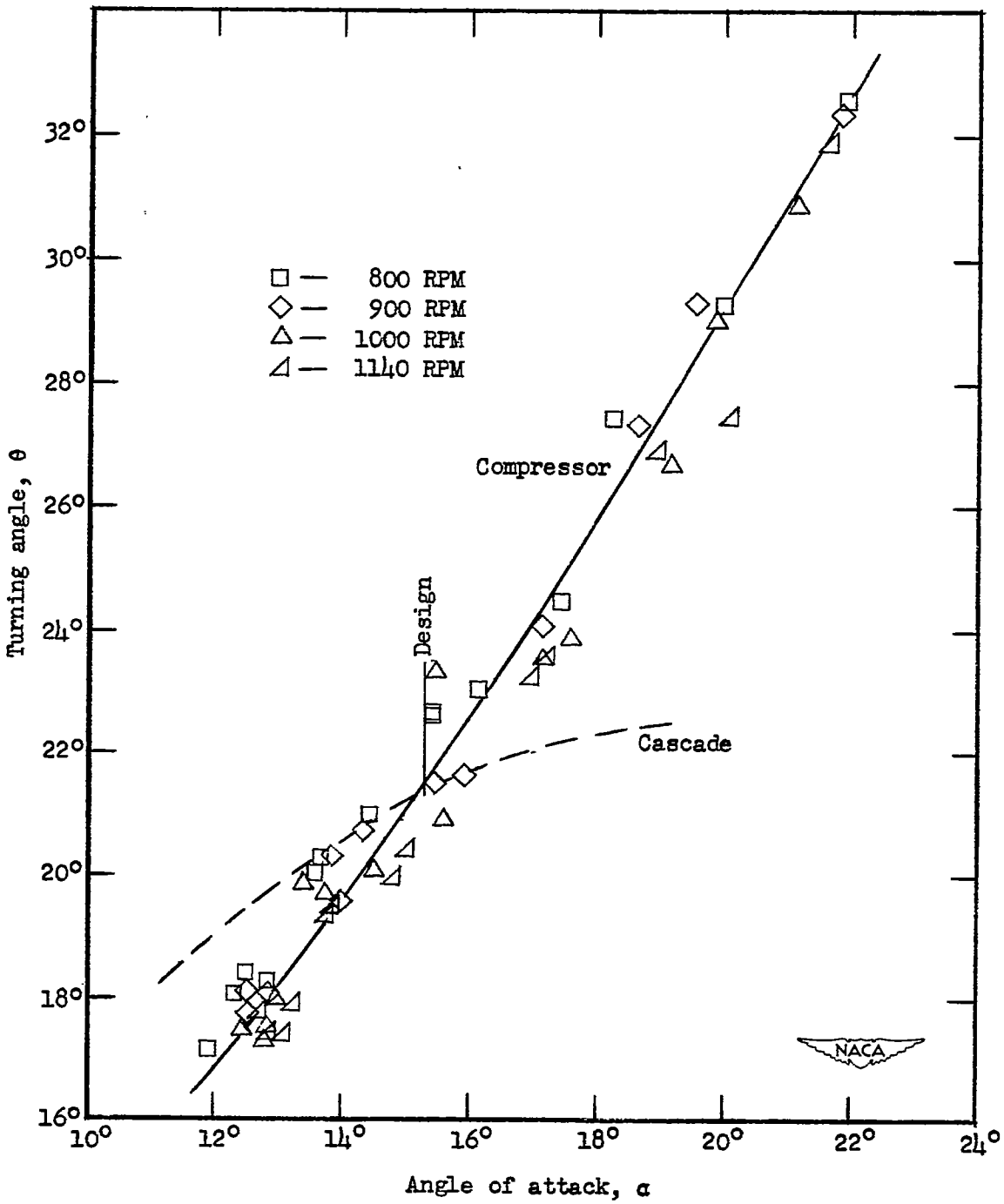

(c) At the inboard section.

Figure 12.- Concluded.

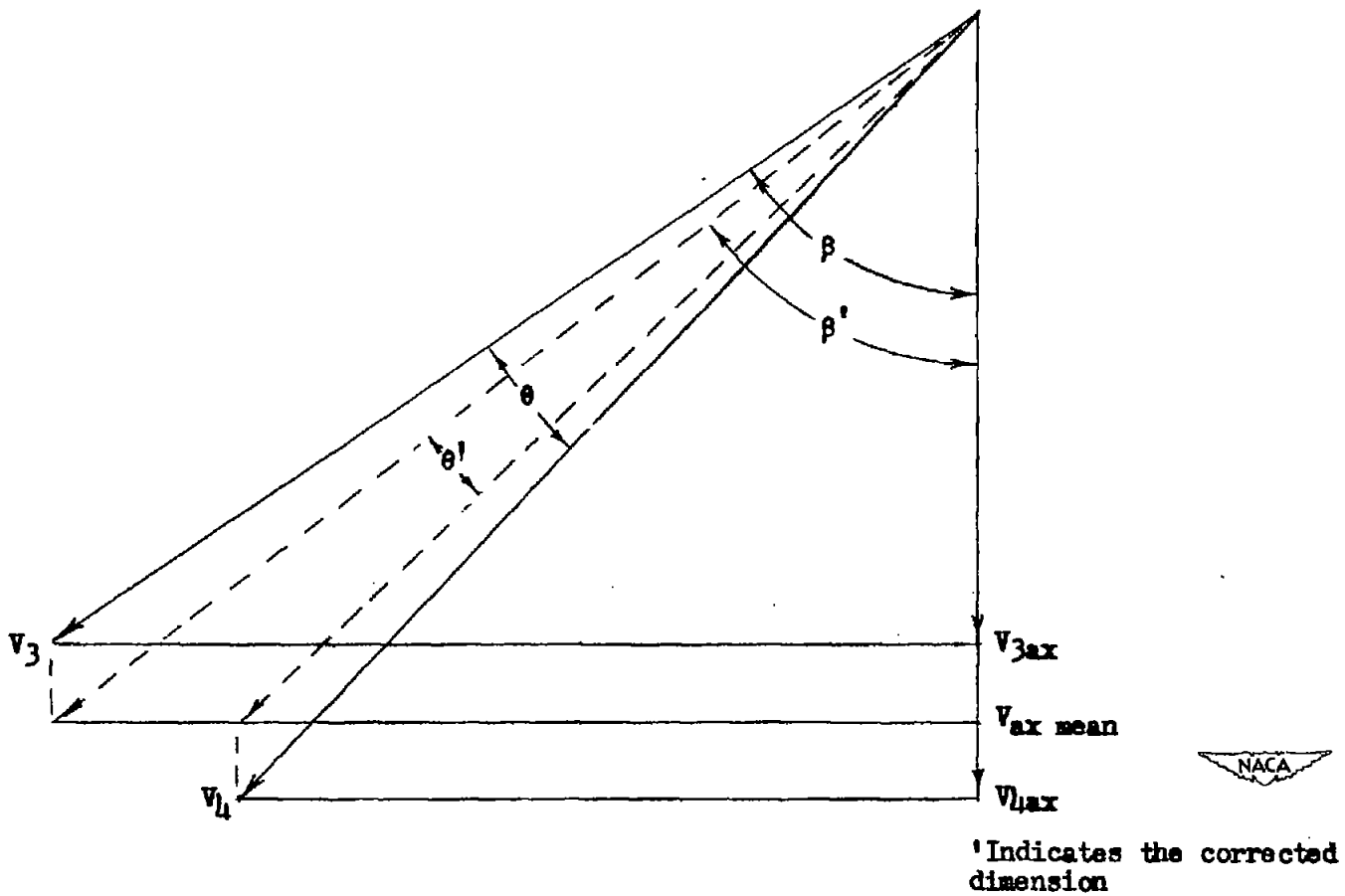

Figure 13.- A vector diagram demonstrating the method of correcting the air angles by using a mean axial velocity.

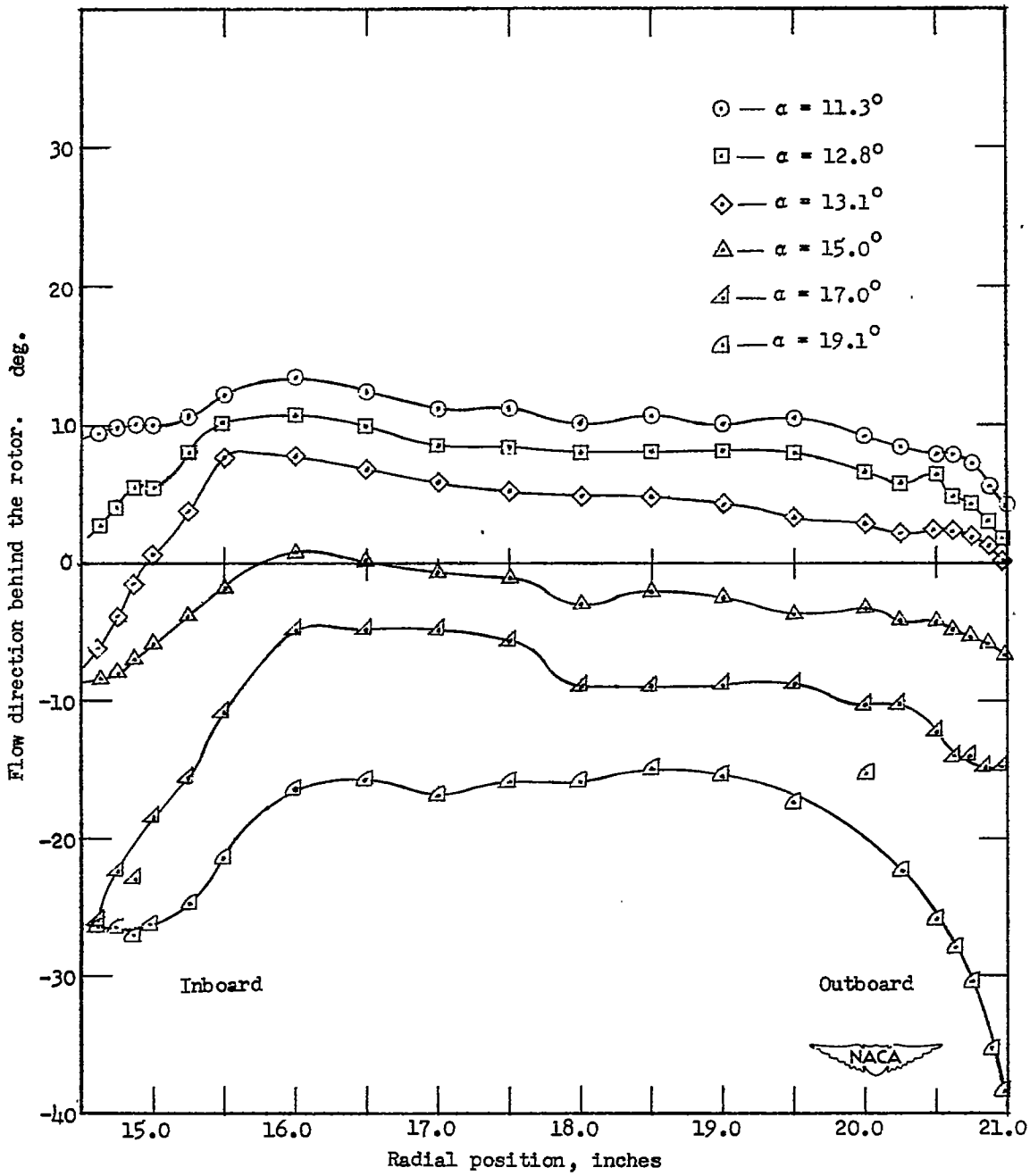

Figure 14.- Flow direction behind the rotor for various angles of attack at mean section.

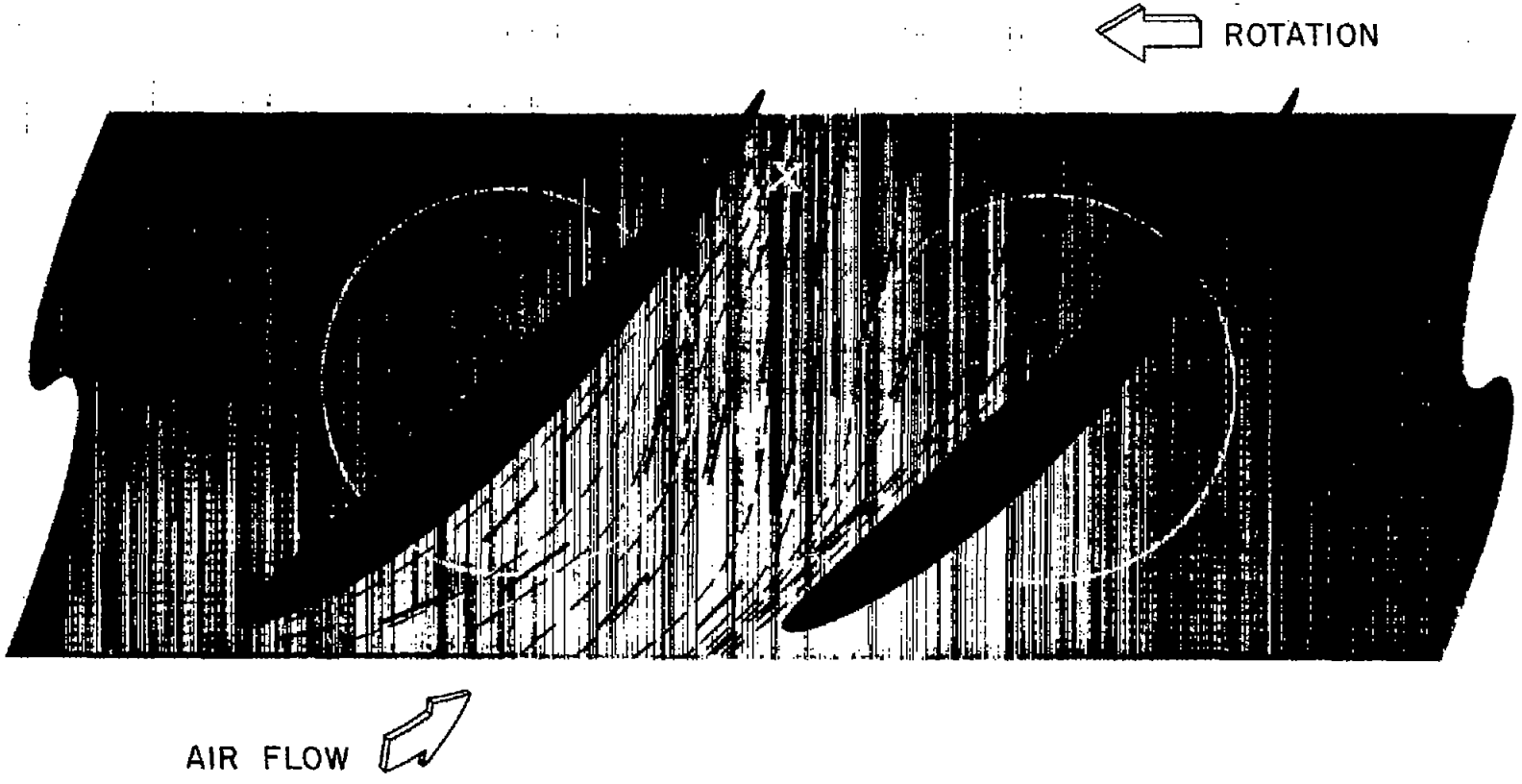

L-67735

(a) Boundary flow at rotor hub as indicated by tufts near design angle of attack.

Figure 15.- Tuft patterns.

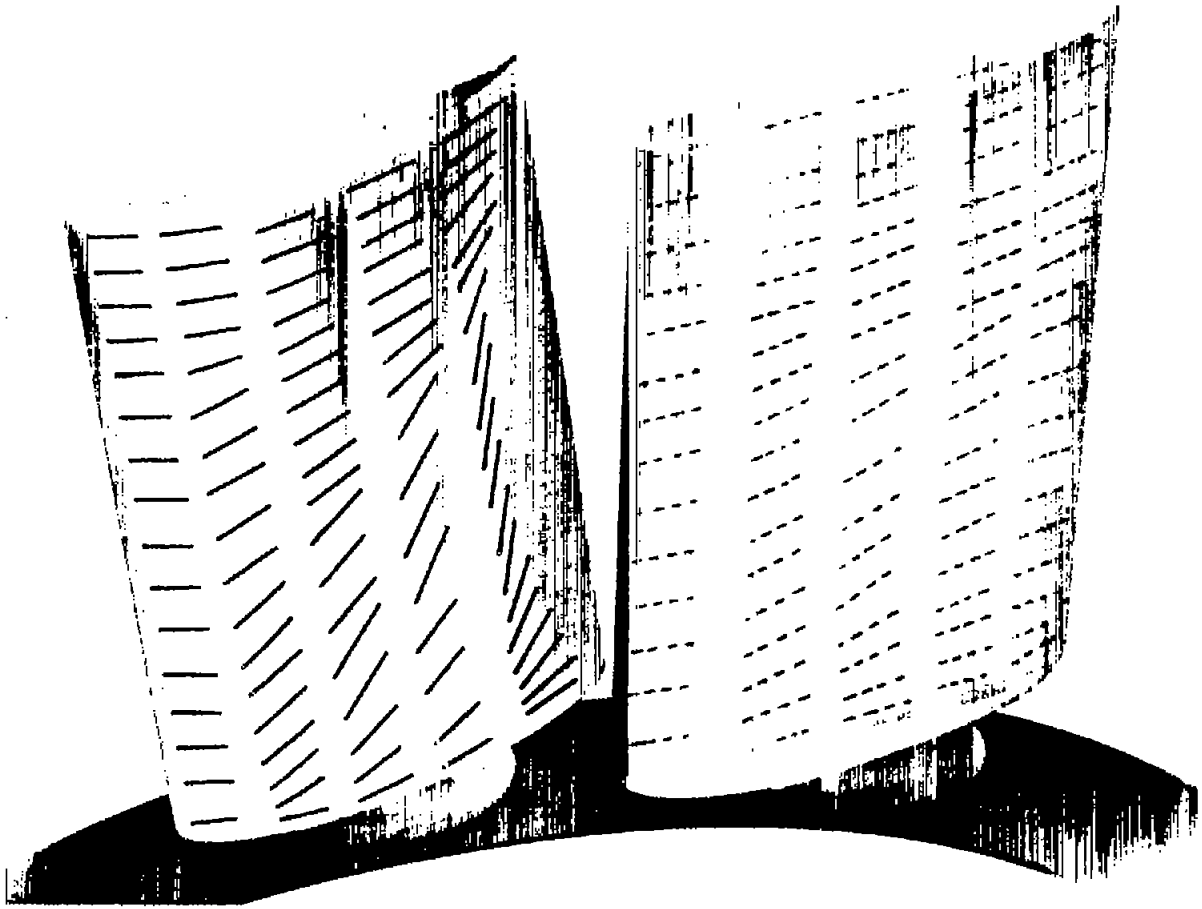

L-67736

(b) Sketch of tufts on rotor blades demonstrating the radial flow of the boundary layer near the design angle of attack.

Figure 15.- Concluded.

(a) Flow behind the rotor in rotating coordinates.

Figure 16.- Wake patterns.

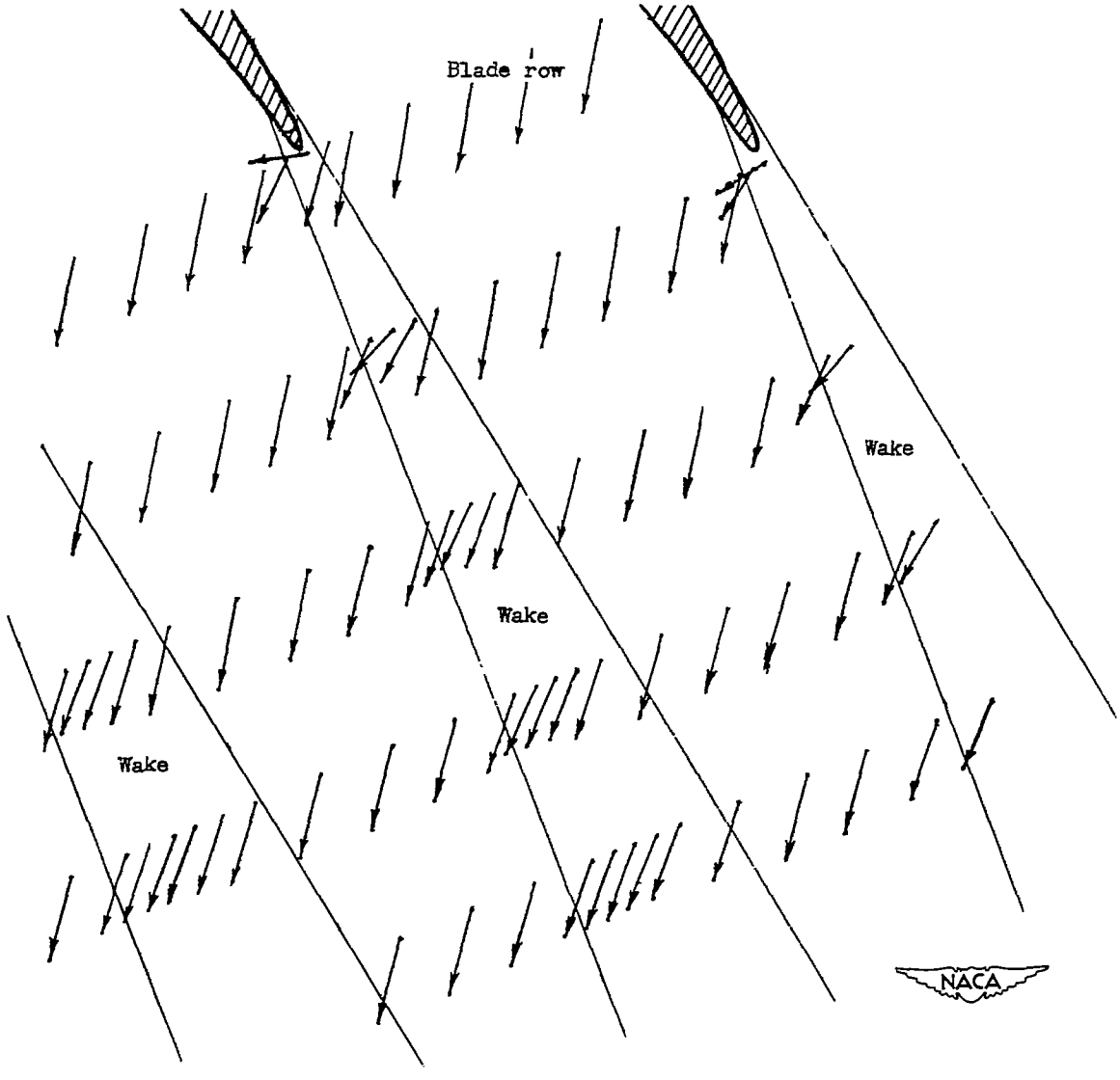

(b) Velocity distribution behind the rotor in stationary coordinates.

Figure 16.- Continued.

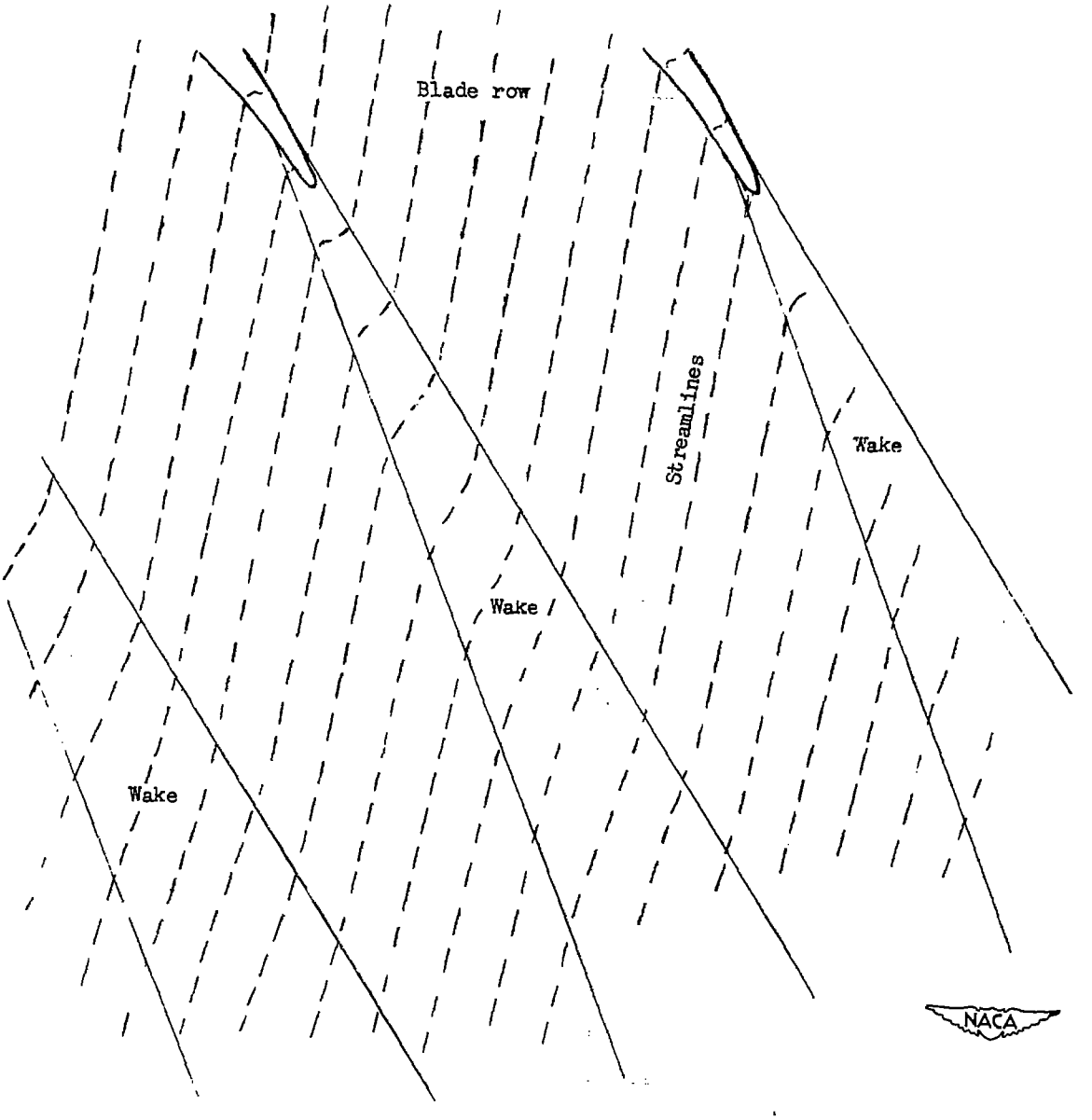

(c) Flow behind the rotor in stationary coordinates.

Figure 16.- Concluded.

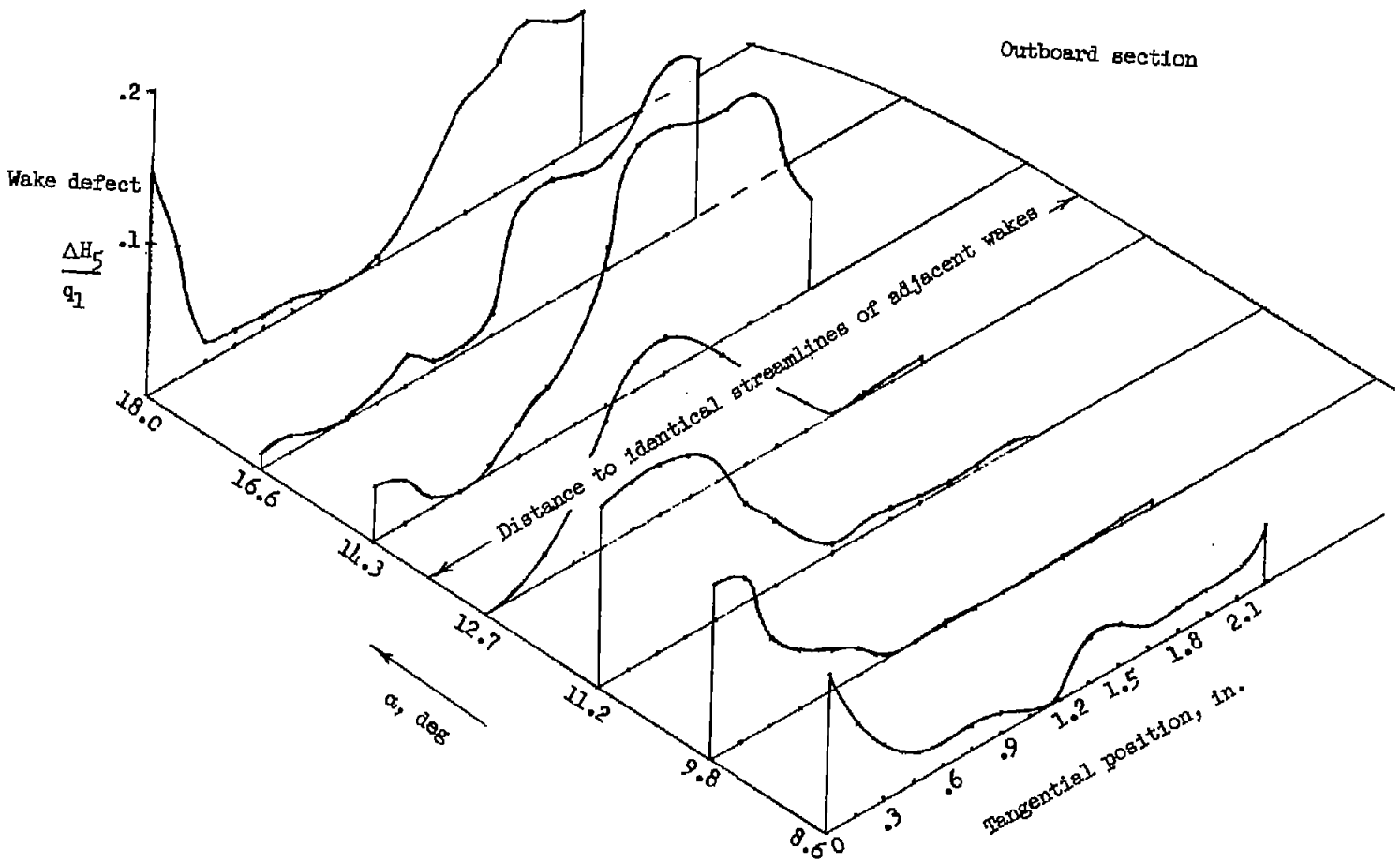

(a) Outboard section

Figure 17.- Guide-vane wakes at station III for several angles of attack.

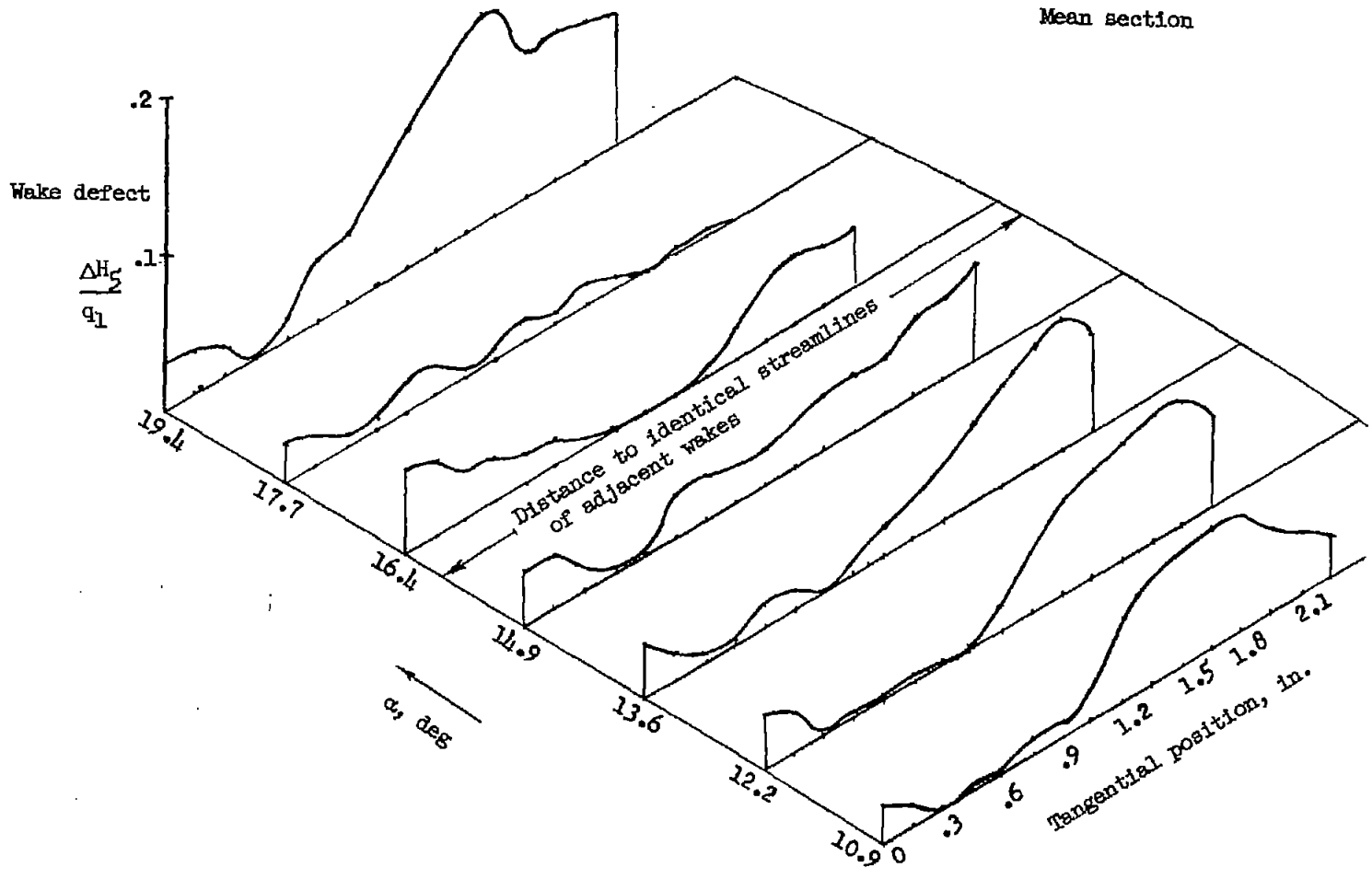

(b) Mean section.

Figure 17.- Continued.

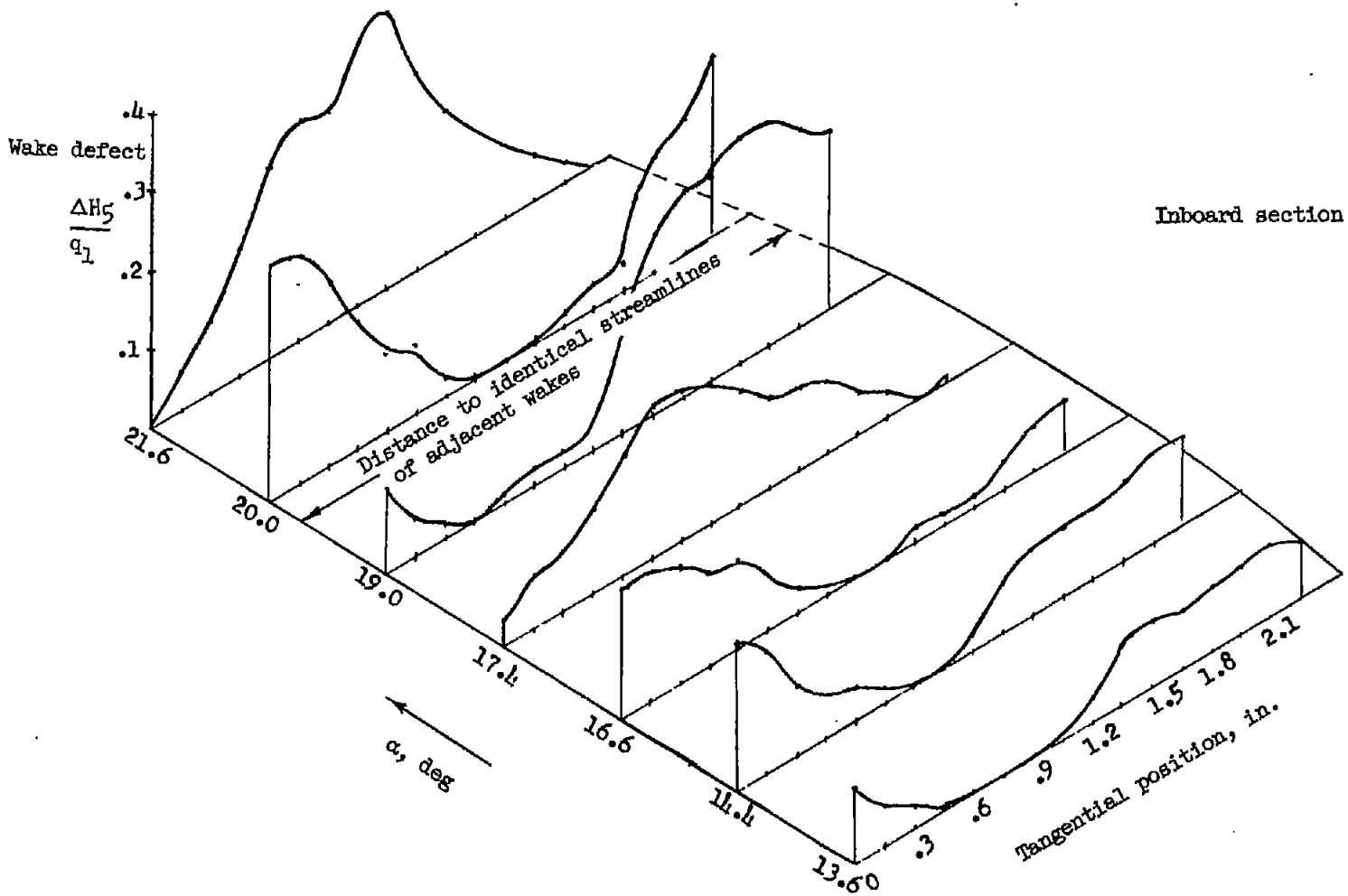

(c) Inboard section.

Figure 17.- Concluded.

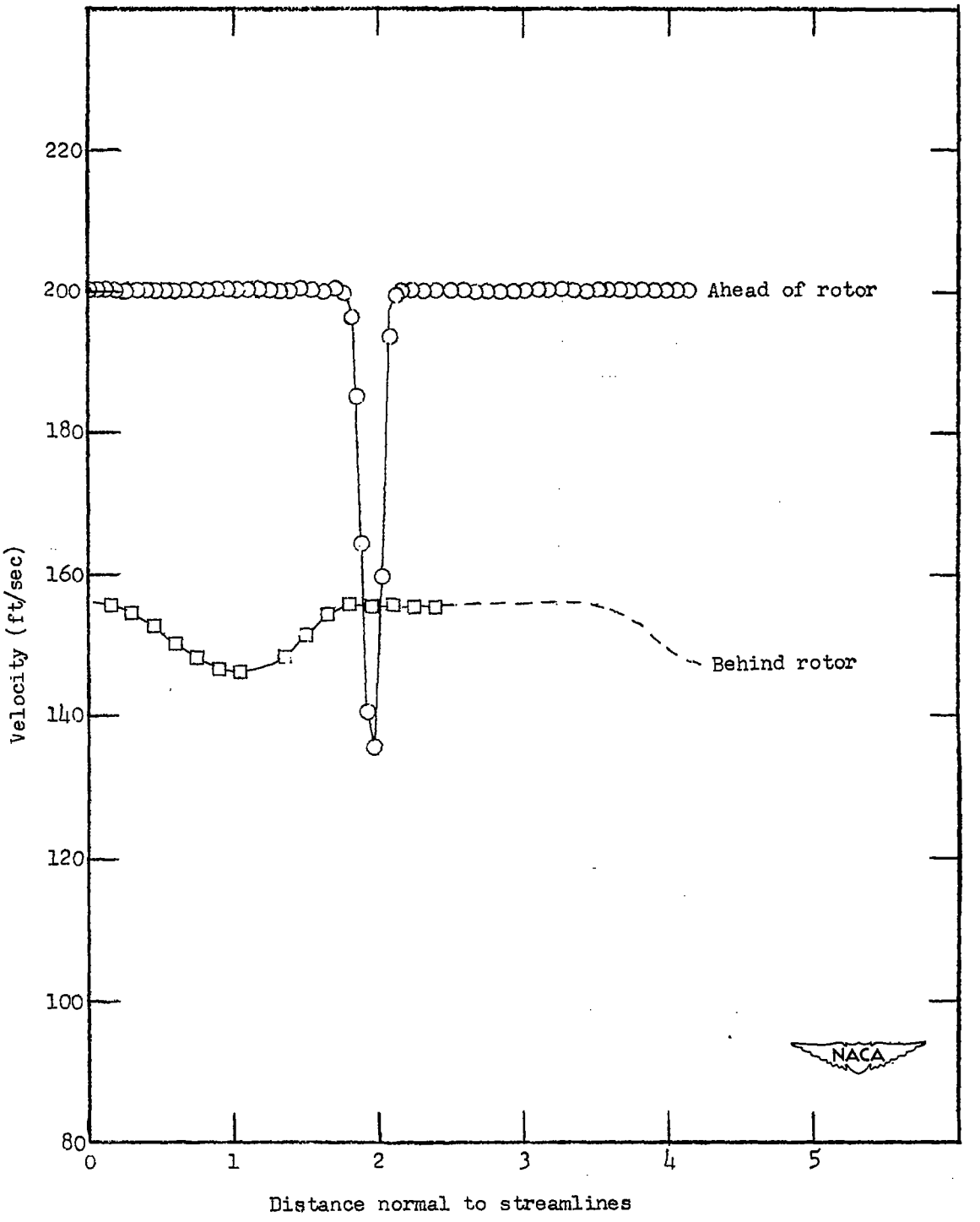

(a) Rotor blade angle of attack of 12.7°, at the outboard section.

Figure 18.- Change in guide-vane wakes on passing through the rotor.

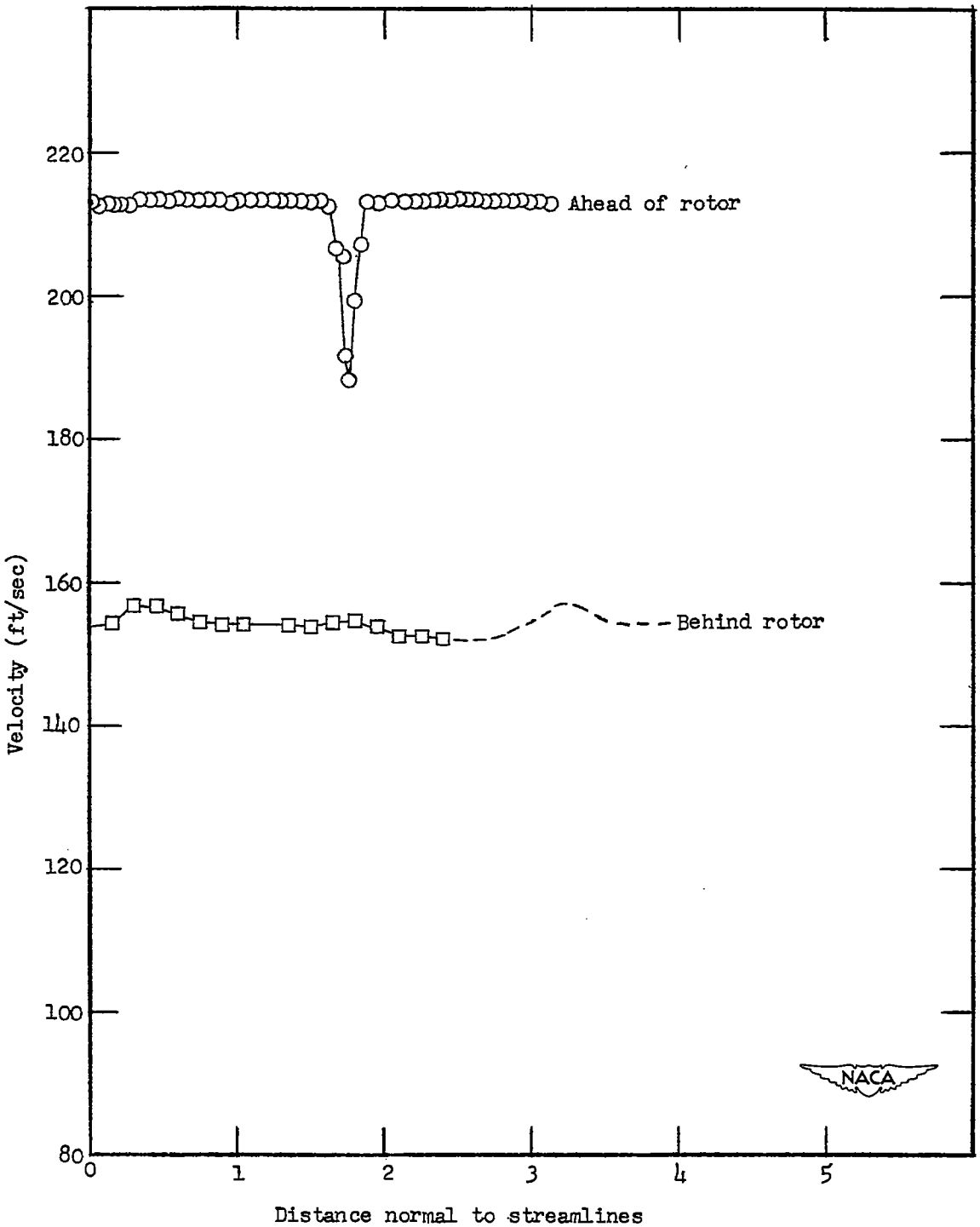

(b) Rotor blade angle of attack of 14.9°, at the mean section.

Figure 18.- Continued.

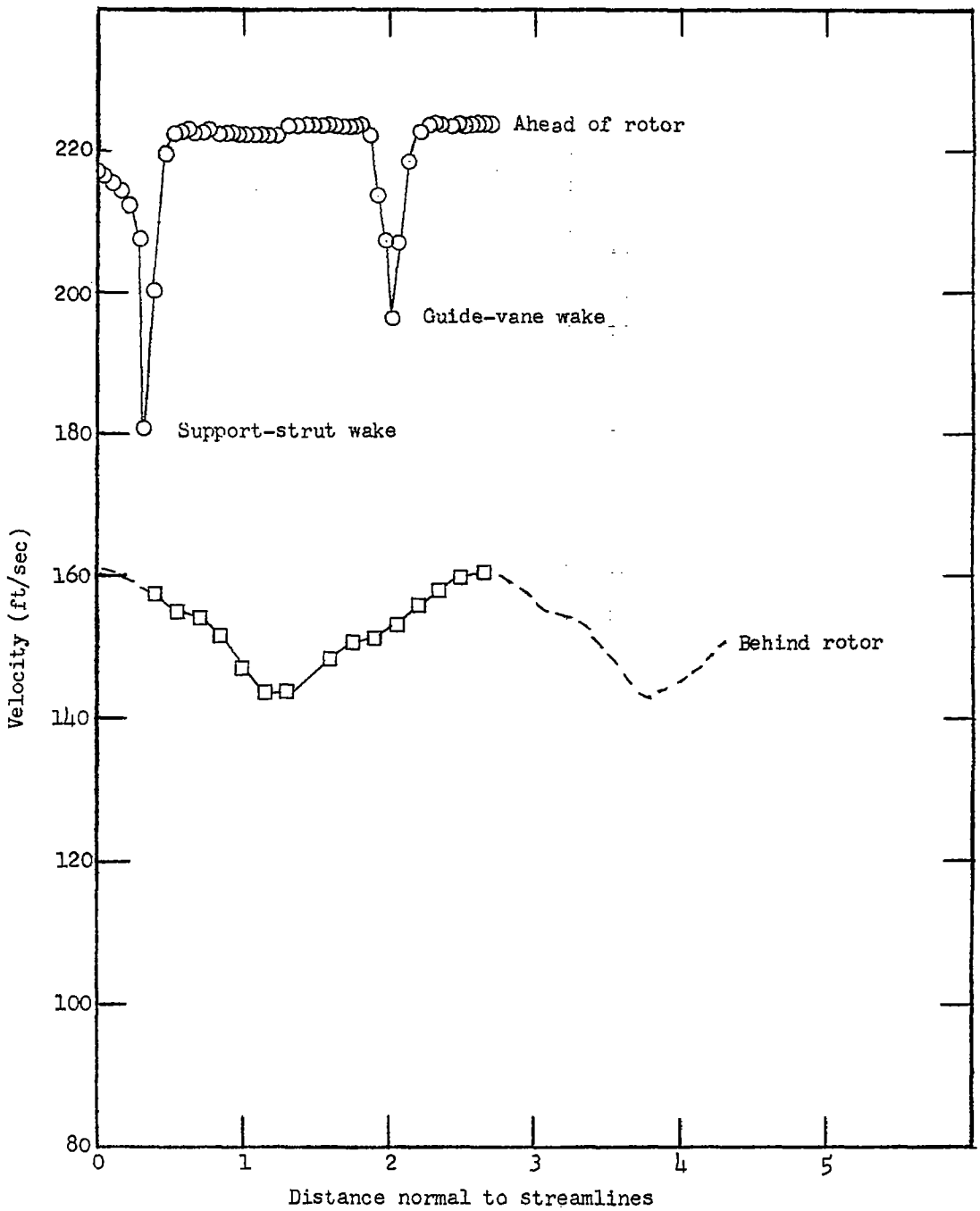

(c) Rotor blade angle of attack of 17.4°, at the inboard section.

Figure 18.- Concluded.

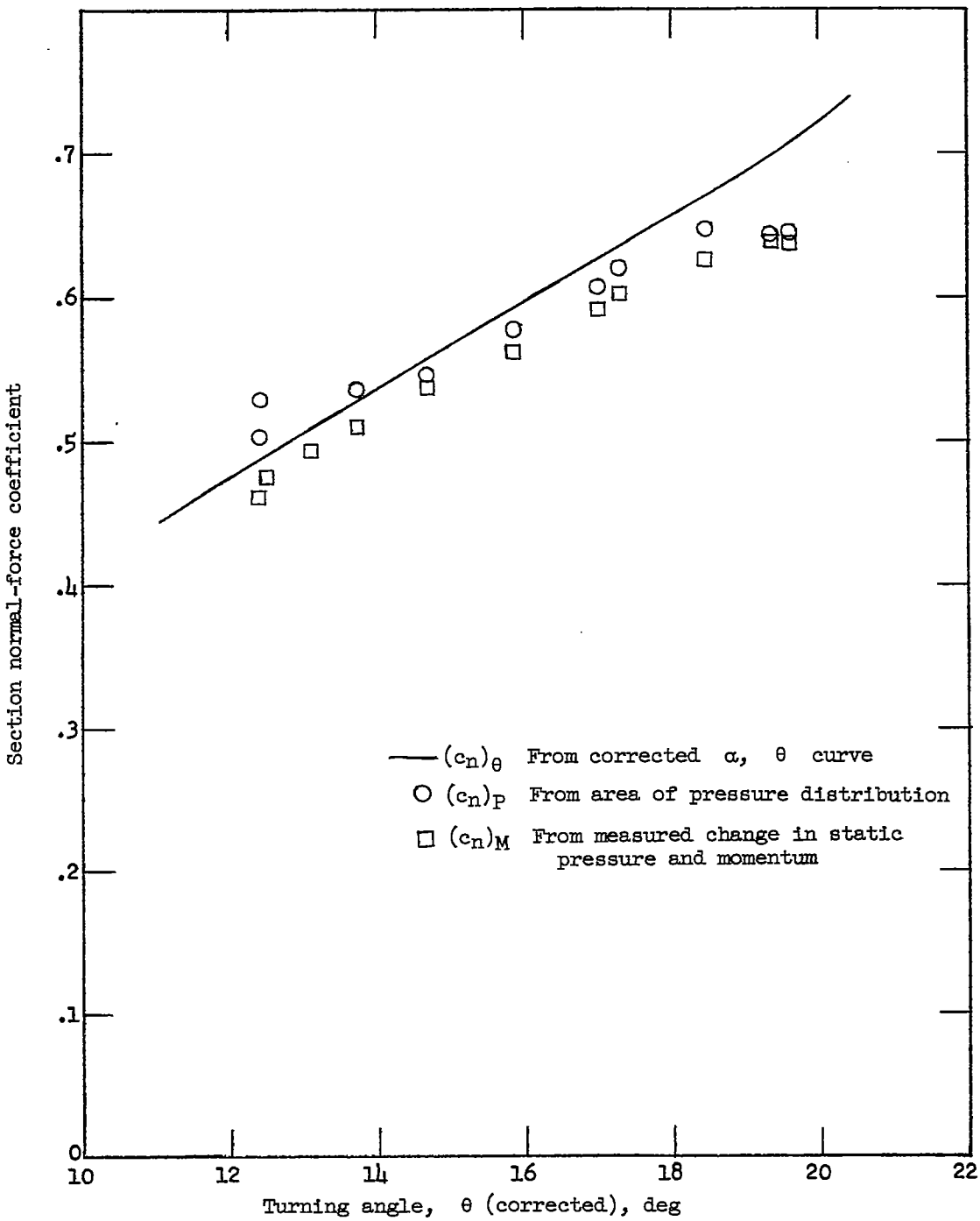

(a) Outboard section.

Figure 19.- Section normal-force coefficient against turning angle.

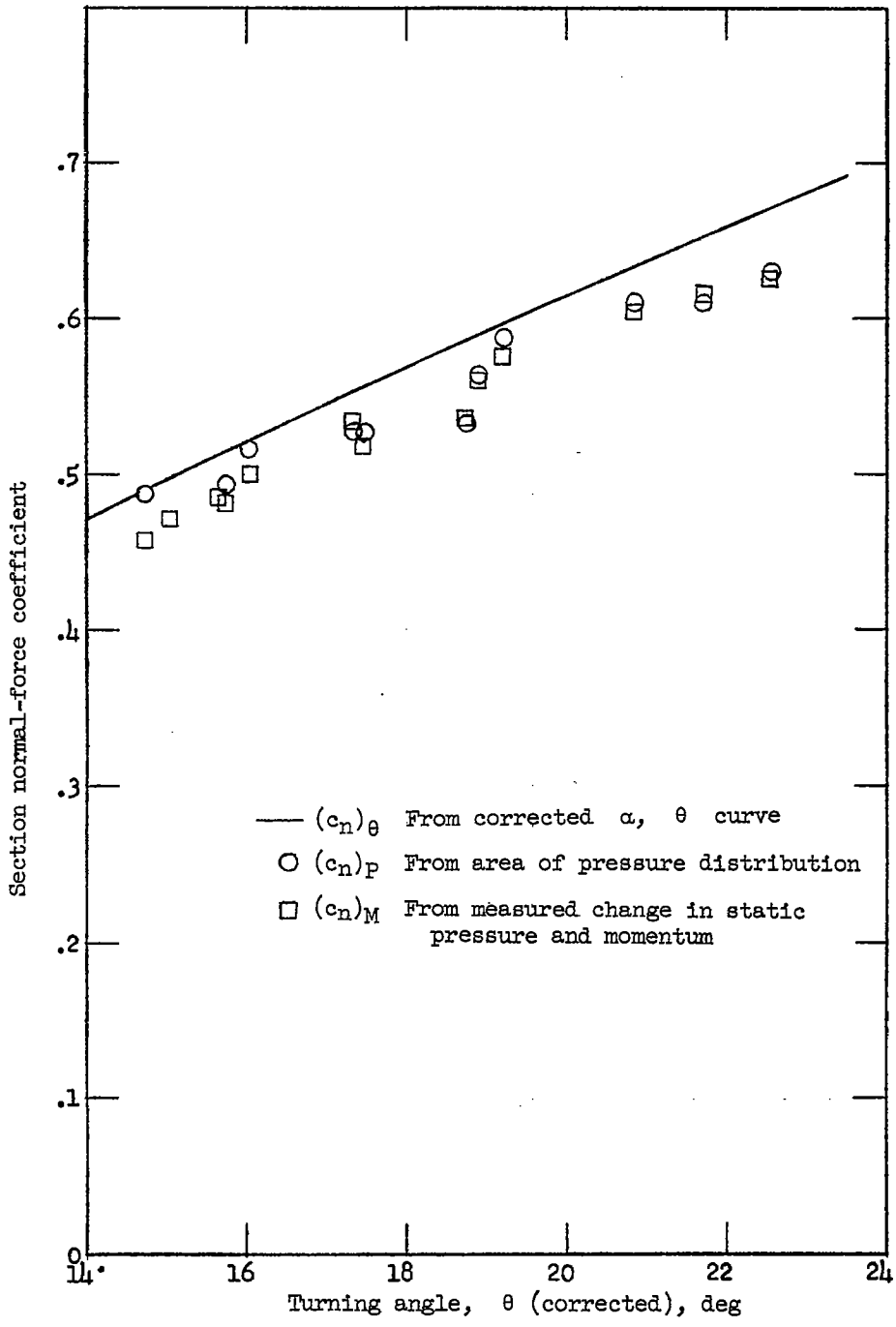

(b) Mean section.

Figure 19.- Continued.

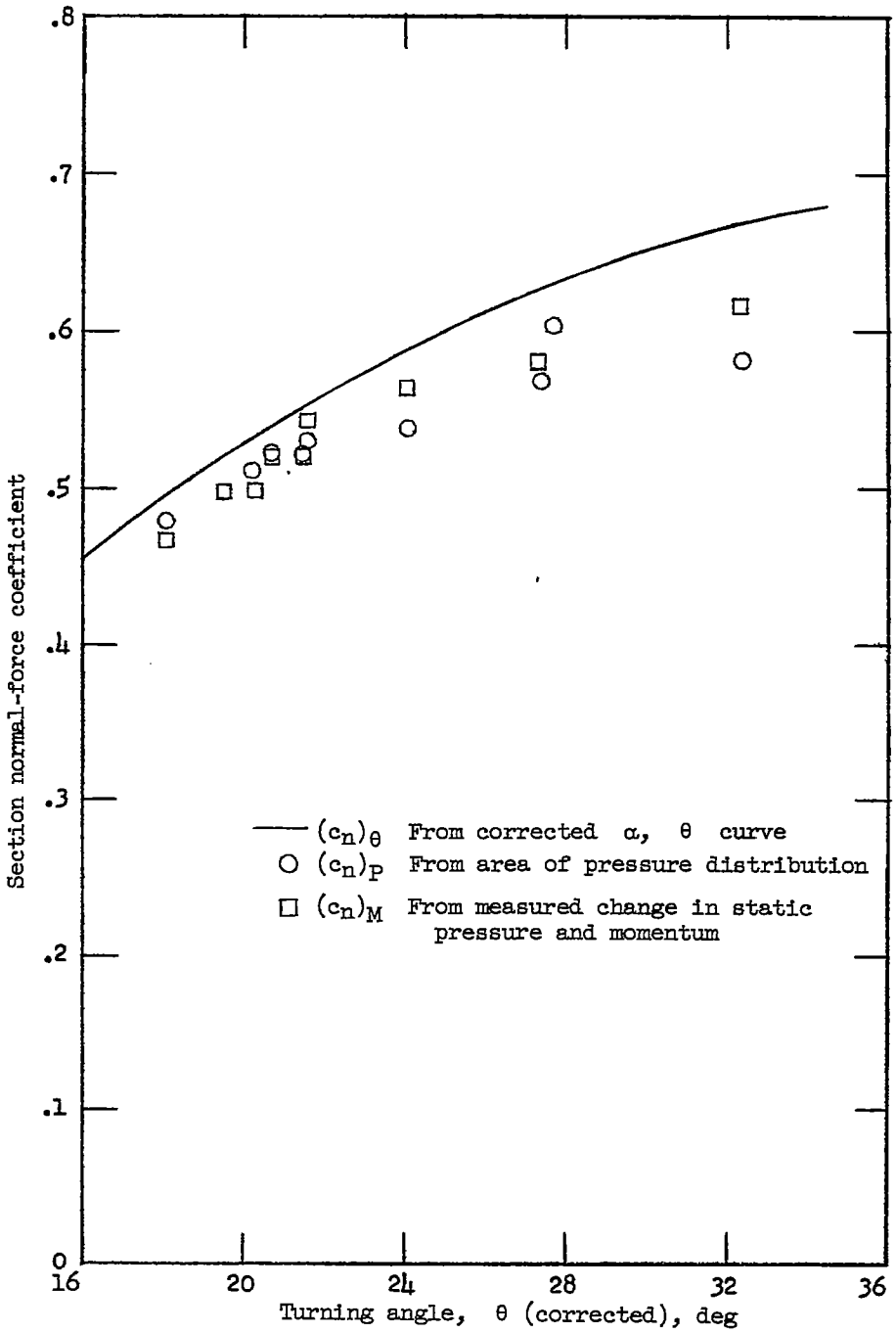

(c) Inboard section.

Figure 19.- Concluded.